RESEARCH ARTICLE

VOLCANICA

Holocene volcanism at the Quetrupillán Volcanic Complex (39°30' S, 71°43' W), southern Chile

Isla C. Simmons*[α], Dave McGarvie[β], Joaquín A. Cortés[α, γ], Eliza S. Calder[α], Andrés Pavez[δ]

[α] School of GeoSciences, University of Edinburgh, Edinburgh, UK
[β] Lancaster Environment Centre, Lancaster University, Lancaster, UK
[γ] Department of Geography, Edge Hill University, Ormskirk, UK
[δ] GEO-3, Chile

Abstract

This paper provides the first detailed description of Holocene volcanism at the Quetrupillán Volcanic Complex. This volcanic complex consists of a truncated and eroded stratocone plus sixteen well-preserved satellite vents on its lower flanks. Intense scouring of the stratocone's flanks (presumably by ice) has removed much evidence of its Holocene eruptions, and thus the Holocene construction of the stratocone (i.e. number and volume of eruptions) cannot be determined. The sixteen satellite vents are the products of an uncertain number of eruptions, with trachyte comprising ~97% of the lava erupted. Geochemical analysis of tephra layers from three logged sections in nearby valleys provides evidence of three explosive eruptions from Quetrupillán. In these sections, no evidence of pyroclastic density current deposits was identified, which may suggest that explosive volcanic hazards from Quetrupillán are less than indicated on current hazard maps.

Keywords: `Holocene; Volcanism; Chile; Trachyte; Glacier-volcano interactions`

1 Introduction

The Quetrupillán Volcanic Complex (Complejo Volcánico Quetrupillán), henceforth shortened to Quetrupillán, lies in the Southern Volcanic Zone of the Chilean Andes, with the stratocone summit (elevation 2360 m) located at 39°30' S, 71°43' W (Figure 1). Unlike its prominent neighbouring volcanoes, Villarrica and Lanín, Quetrupillán is somewhat hidden from view, and this may explain why there is uncertainty over whether there have been any eruptions from Quetrupillán since the surrounding valleys were first settled by the Spanish in the mid-16th century. For example, Quetrupillán cannot be seen from the main settlements of either Villarrica or Pucón as it is hidden behind Volcán Villarrica. The last eruption from Quetrupillán is suspected to have occurred in 1872 CE [Petit-Breuilh Sepúlveda 2004], but we consider the evidence for this weak, as it lacks corroboration from multiple independent sources.

Past work on Quetrupillán has been sporadic, and a detailed geological map of the volcanic complex has not been published. Consequently, the volcanic stratigraphy is unknown. Only reconnaissance-level mapping has been carried out and results were presented at conferences [Pavez 1997], but not in peer-reviewed journals. Likewise, a study of volcano-ice interactions during the late Pleistocene began in 2012 but has only appeared in conference presentations [e.g. McGarvie 2014]. A study of tephra layers in the nearby Trancura Valley that have been attributed to explosive eruptions at Quetrupillán was the subject of a dissertation [Toloza 2015]. Most recently, Brahm et al. [2018] conducted a study that analysed a limited subset of Holocene trachytic lavas.

The volcanic complex of Quetrupillán consists of a truncated (headless) stratocone, and numerous satellite vents around the lower flanks of the stratocone, particularly on the southern flank (Figure 2). Two areas of distal volcanism are speculated to be satellite vents of Quetrupillán: Huililco, a small basaltic andesite scoria cone ~12 km to the northeast, and Llizan, a cluster of vegetated scoria cones ~14 km to the SSW (Figure 1; Brahm et al. [2018]; Pavez [1997]; Sun [2001]; Valdivia Muñoz [2016]). Given that their relationship to Quetrupillán is currently both uncertain and unproven, we do not consider these further in this paper.

The aims of this study are to: (1) map Holocene volcanism at Quetrupillán, so as to understand the pattern of eruptive activity; (2) analyse lavas and pyroclastics, so as to understand the range of compositions erupted; (3) log pyroclastic deposits in nearby valleys in order to establish the wider distribution and effects of explosive eruptions; and (4) synthesise the information obtained in (1–3) and use this to evaluate hazards from future eruptions of Quetrupillán.

*Corresponding author: isla.simmons@ed.ac.uk

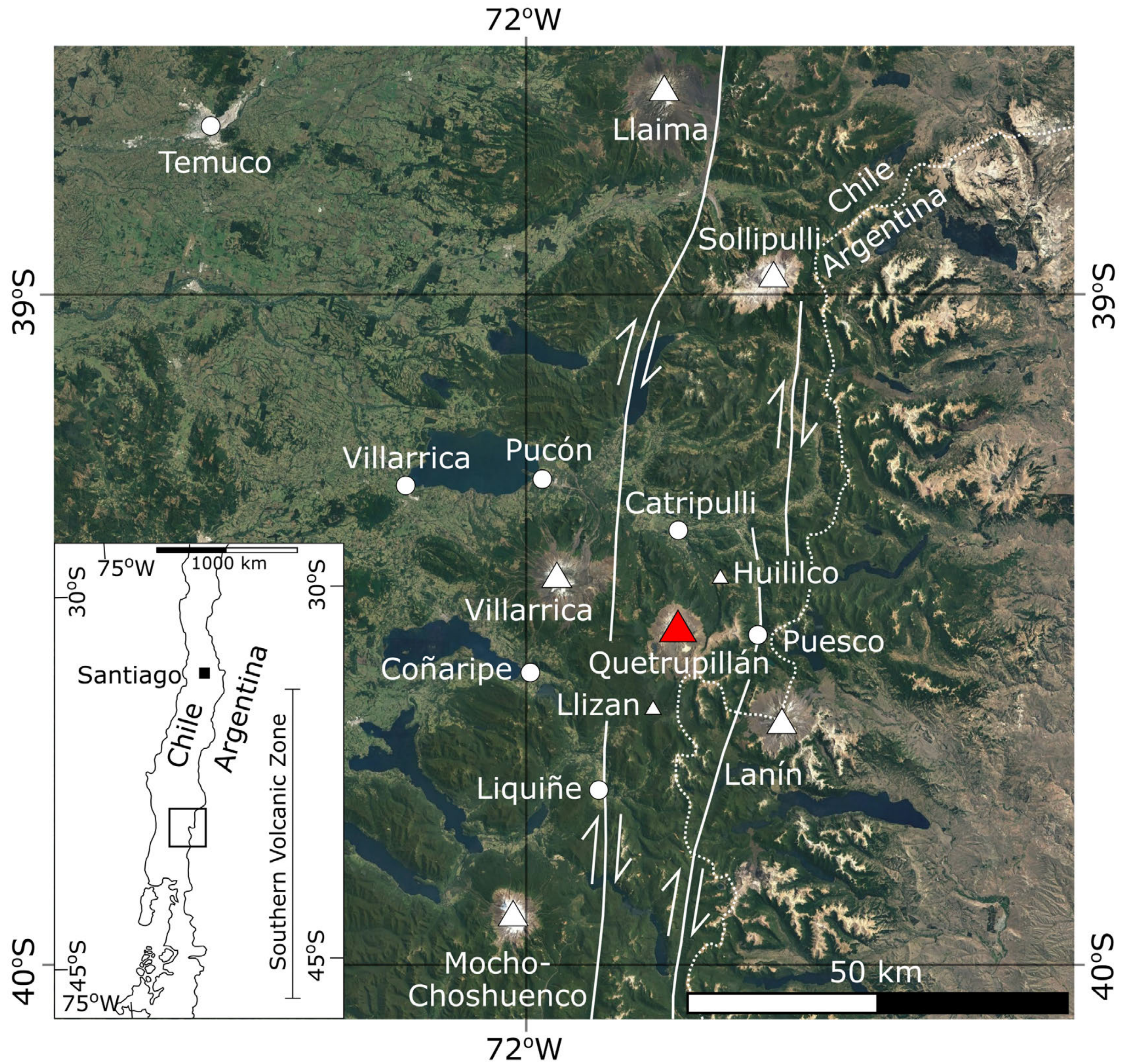

Figure 1: Satellite image of the area surrounding Quetrupillán showing the trace of the Liquiñe-Ofqui Fault Zone faults (solid lines), as mapped by Hernandez-Moreno et al. [2014]. Volcanoes (triangles; Quetrupillán highlighted in red) and settlements (circles; notable towns or those mentioned in this paper) are indicated. Satellite image from Google Earth (downloaded 03/02/2020). Dotted line: international border between Chile and Argentina. The inset shows the location of the region within Chile, and the location of the Southern Volcanic Zone.

2 Regional setting

Along the western edge of South America, the oceanic Nazca Plate is subducting below the continental South American Plate with oblique convergence [Cembrano and Lara 2009; Stern 2004], resulting in the NNE-trending margin-parallel volcanic arc of the Andes. The Southern Volcanic Zone (SVZ) lies between 33°S and 46°S [López-Escobar et al. 1995], where magmatism is controlled primarily by the dehydration of the subducted Nazca Plate and resultant partial melting of the mantle wedge [Cembrano and Lara 2009; Stern 2004; Tatsumi 2005].

The main structural feature of the SVZ is the Liquiñe-Ofqui Fault Zone (LOFZ), a ~1000 km long NNE-trending intra-arc fault system [Cembrano et al. 1996; Hernandez-Moreno et al. 2014] which has been interpreted to act as an active dextral transpressive strike-slip structure for at least the last 6 Ma [Cembrano and Lara 2009]. Quetrupillán sits within the LOFZ (Figure 1), though there is debate on the precise location of the actual LOFZ faults. For example,

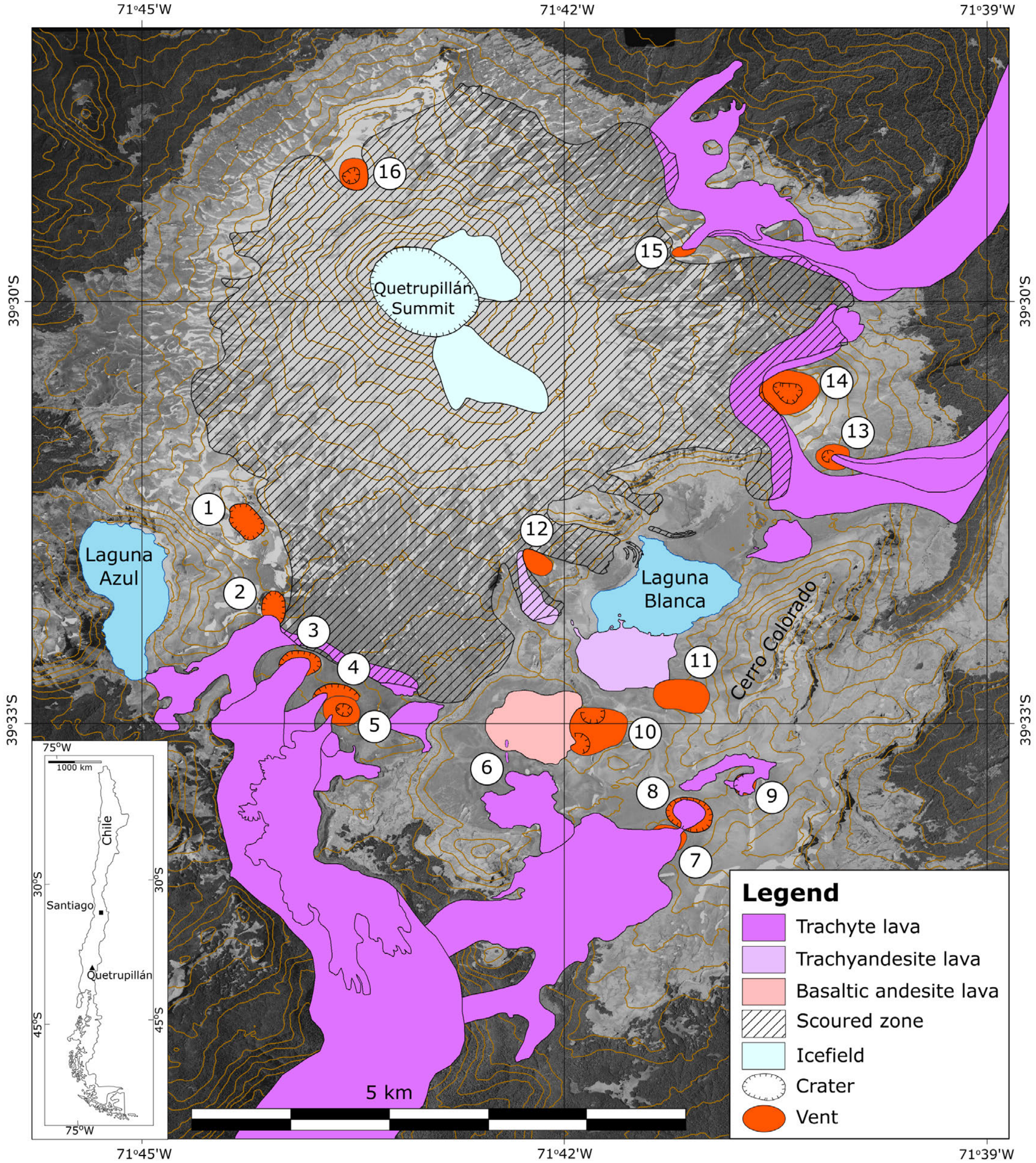

Figure 2: Map of the Holocene geology of Quetrupillán from the satellite flank vents. Satellite vents are labelled with the numbers that they are referred to in the text. The glacially scoured zone is indicated by the area of hatching. The aerial photo background image is from the Servicio Aerofotogramétrico and 50 m interval contours were created from a digital elevation model downloaded from earthexplorer.usgs.gov (downloaded 21/10/2016). The inset shows the location of Quetrupillán in Chile.

Moreno Roa and Lara [2008] map the LOFZ as passing immediately to the west of Quetrupillán, along the Palguin Valley, while Rosenau et al. [2006] map one fault terminating immediately south of Quetrupillán and another along the Trancura Valley to the east. Hernandez-Moreno et al. [2014] map a splay of the LOFZ on either side of Quetrupillán, along the Trancura Valley to the east, and across the eastern flank of

Villarrica to the west. Irrespective of the precise location of LOFZ faults in the area, it is evident that faulting associated with the LOFZ has had a major influence on both the location and triggering of eruptions at Quetrupillán [McGarvie 2014].

Quetrupillán sits within the NW–SE orientated Villarrica-Quetrupillán-Lanín volcanic chain (Figure 1 and Figure 3), a chain of three active volcanoes, that lies oblique to the main volcanic arc of the Andes [Cembrano and Lara 2009; Hickey-Vargas et al. 1989]. Villarrica (39°25' S, 71°56' W), the westernmost volcano, is one of the most active volcanoes in South America [Petit-Breuilh Sepúlveda 2004]. It is an ice-capped, basaltic andesite stratocone with persistent open-vent degassing from the lava lake in its summit crater [Witter et al. 2004]. The easternmost volcano is the basalt-to-dacite stratocone of Lanín (39°38' S, 71°30' W), which has not had any recorded historic eruptions [Lara et al. 2004] and which has a small summit ice cap. Quetrupillán lies between Villarrica and Lanín, and its truncated stratocone contrasts strongly with the conical stratocones of Villarrica and Lanín (Figure 3).

Quetrupillán has been constructed on a basement of Cretaceous and Miocene plutonic units and Triassic to Miocene volcano-sedimentary sequences of the Panguipulli, Curarrehue and Trapatrapa Formations [Moreno Roa et al. 1994]. It has been suggested that Quetrupillán overlies the eroded remnants of the unstudied and undated (Pleistocene?) stratovolcanoes of Quinquilil (also known as "Colmillo del Diablo") and Cordillera El Mocho [Pavez 1997].

3 Methods

Two field seasons were conducted at Quetrupillán, in February 2017 and January 2018. Observations of deposits were made, samples were collected from lava flows and pyroclastic sequences, and field mapping was supplemented with satellite images. In total, 70 samples were collected from lava flows on the flanks of Quetrupillán, and 48 pyroclastic deposits were sampled in the Palguin and Trancura valleys, to the northwest and east of Quetrupillán, respectively.

All further analyses were undertaken at the University of Edinburgh. Polished thin sections of 36 samples of Holocene lavas were cut, and these were analysed under a petrological microscope. Twenty-one thin sections were studied using the scanning electron microscope (SEM) and semi-quantitative analyses were performed using the energy dispersive spectrometer (EDS) included in the instrument [https://www.ed.ac.uk/geosciences/facilities/sem/specification]. Thirteen thin sections were further analysed with the electron microprobe (EMPA) [https://www.ed.ac.uk/geosciences/facilities/electron/instrumentspec].

Fifty-seven samples of Holocene lavas and pyroclastic deposits were selected for X-ray fluorescence (XRF) analysis [https://www.ed.ac.uk/geosciences/facilities/xrayfluorescence/xrf] to determine abundances of major and trace elements. Samples were crushed and then ground to powder using agate grinding jars. Trace element concentrations were measured from pressed powder pellets. Major element concentrations were measured from fused glass discs. To create the discs, powders were heated at 1100 °C for 20 min and the loss on ignition (LOI) of volatiles was recorded (tephra samples were first heated overnight at 450 °C to burn off any organic material). Powders were then mixed with a borate flux and remelted at 1100 °C, before casting on a hotplate.

4 Holocene Volcanism at Quetrupillán

4.1 Introduction

As a volcanic stratigraphy corroborated by absolute age dating has not been established for Quetrupillán, care needs to be taken when assigning volcanic features to a particular epoch. In southern Chile the last glacial period is known as the Llanquihue (29,400–14,550 ^{14}C yr BP; Glasser et al. [2008]), with the last glacial maximum (LGM) occurring 23,000–19,000 cal yr ago, when ice covered the crest of the Andes for ~1800 km [Hulton et al. 2002]. At Quetrupillán, the ice would have been at least 500 m thick, and possibly as thick as 1300 m [Hulton et al. 2002]. Deglaciation started ~17,500–17,150 cal yr ago with abrupt and stepped warming resulting in a dramatic reduction of the ice mass covering the Andes in this part of Chile [Hulton et al. 2002; Moreno et al. 1999]. Glacial retreat was rapid, and within ~2000 years glaciers in this region had receded to within 10 km of their current termini [Lowell et al. 1995].

Given the above, any lava at Quetrupillán that clearly shows the combined evidence of ice confinement and of ice/meltwater-induced cooling fracture systems (characteristic of intermediate-silicic glaciovolcanic eruptions, e.g. McGarvie [2009]) is assumed to have erupted when ice covered the area, and is assigned a Pleistocene age [McGarvie 2014]. In contrast, any lava that demonstrates the typical subaerial characteristics of (unconfined) spreading across the landscape, plus preservation of 'delicate' features (e.g. loose, blocky carapaces), is assigned a Holocene age. This simple two-fold classification scheme has been used at other Chilean volcanoes such as Nevados de Chillán [Dixon et al. 1999], and the nearby volcanoes of Villarrica and Lanín [Lara et al. 2004; Moreno Roa et al. 1994].

One issue with this simple two-fold classification is that local ice masses increased during the Little Ice Age (~14th–19th century; Matthews and Briffa [2005]), and thus Holocene eruptions during this period would have encountered ice and acquired the characteristics

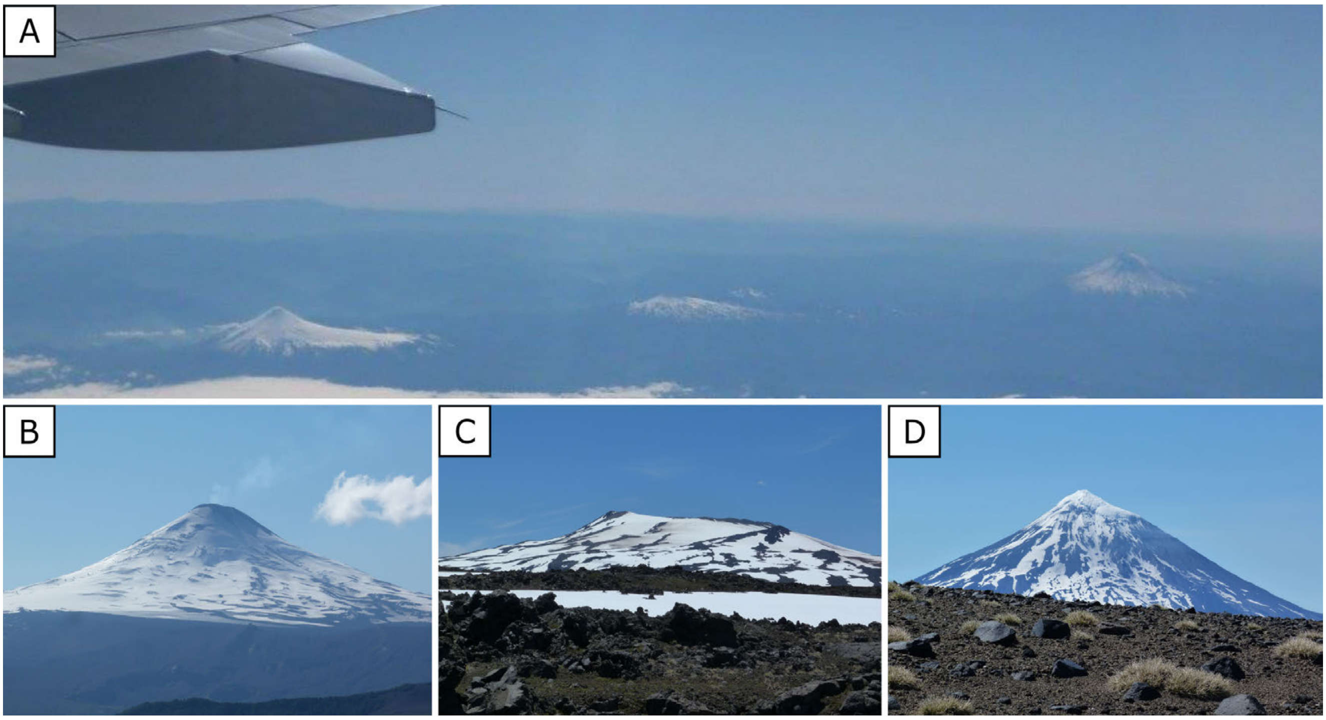

Figure 3: [A] The Villarrica-Quetrupillán-Lanín volcanic chain (looking northeast) with Villarrica [B] to the left, Quetrupillán [C] in the middle and Lanín [D] to the right. The difference in morphology between the conical volcanoes of Villarrica and Lanín and the truncated stratocone of Quetrupillán is clearly visible. The distance between the summits of Villarrica and Lanín is ~45 km.

of glaciovolcanic eruptions. A consequence of this is that lavas may have been assigned a Pleistocene age when in fact they are Holocene, leading to an under-reporting of Holocene erupted volumes. No study that we are aware of has addressed this issue at a Chilean volcano.

At Quetrupillán, we assign a Holocene age to lavas and pyroclastic edifices that have clear and well-preserved subaerial features. An interglacial age is ruled out on the grounds that substantial erosion by the thick ice of the Llanquihue glaciation [Denton et al. 1999; Hulton et al. 2002] would have removed loose material such as scoria and blocky lava carapaces.

4.2 Holocene glacier-volcano interactions

Currently, icefields of unknown thickness occur on the upper parts of the stratocone (Figure 2), with the main ice mass occupying the oval ~1.3 × 1 km summit crater and having an ice surface that dips gently to the southeast. The summit crater has walls of variable height, and at two low points ice has flowed out to form a small (~0.8 × 0.4 km) icefield to the northeast and another to the southeast (~1.4 × 0.7 km).

Surrounding the stratocone and extending some 2–5 km from the summit is a zone that we call the scoured zone (Figure 2), within which all exposed lavas surfaces are smooth and etched with parallel linear scratches and gouges (Figure 4A), and covered by an impersistent blanket of diamict (Figure 4B and 4C). Etching directions can be determined both on a micro scale from scratches on smooth lava surfaces (Figure 4A), and on a macro scale from satellite imagery in which irregular linear channels are eroded into the lava and diamict deposits (Figure 5A). All micro and macro direction indicators are oriented radially to the stratocone summit.

The diamict blanket is a poorly sorted and unconsolidated deposit consisting of sub-rounded to sub-angular lava boulders of varying size, with a smaller sand-silt sized fraction (Figure 4B). The circumference of the scoured zone is often marked by curved ridges of boulders that form distinct topographic highs (Figure 5B). These are typically ~2 metres high but occasionally reach up to 4 metres in height. Our interpretation of these features is that the scoured zone is the product of glacial processes, with the scratches and gouges being glacial striations produced during ice advance, and the diamict representing glacial till deposition during ice retreat. The ridges of boulders around the circumference are terminal moraines that represent the farthest extent of ice advance.

We rule out the Llanquihue glaciation as being the cause of this scoured zone. During the Llanquihue glaciation, thick (>500 m) ice extended for many tens of km on either side of the Andean chain [Hulton et al. 2002], whereas this scoured zone is a local feature, extending 2–5 km from the summit of Quetrupil-

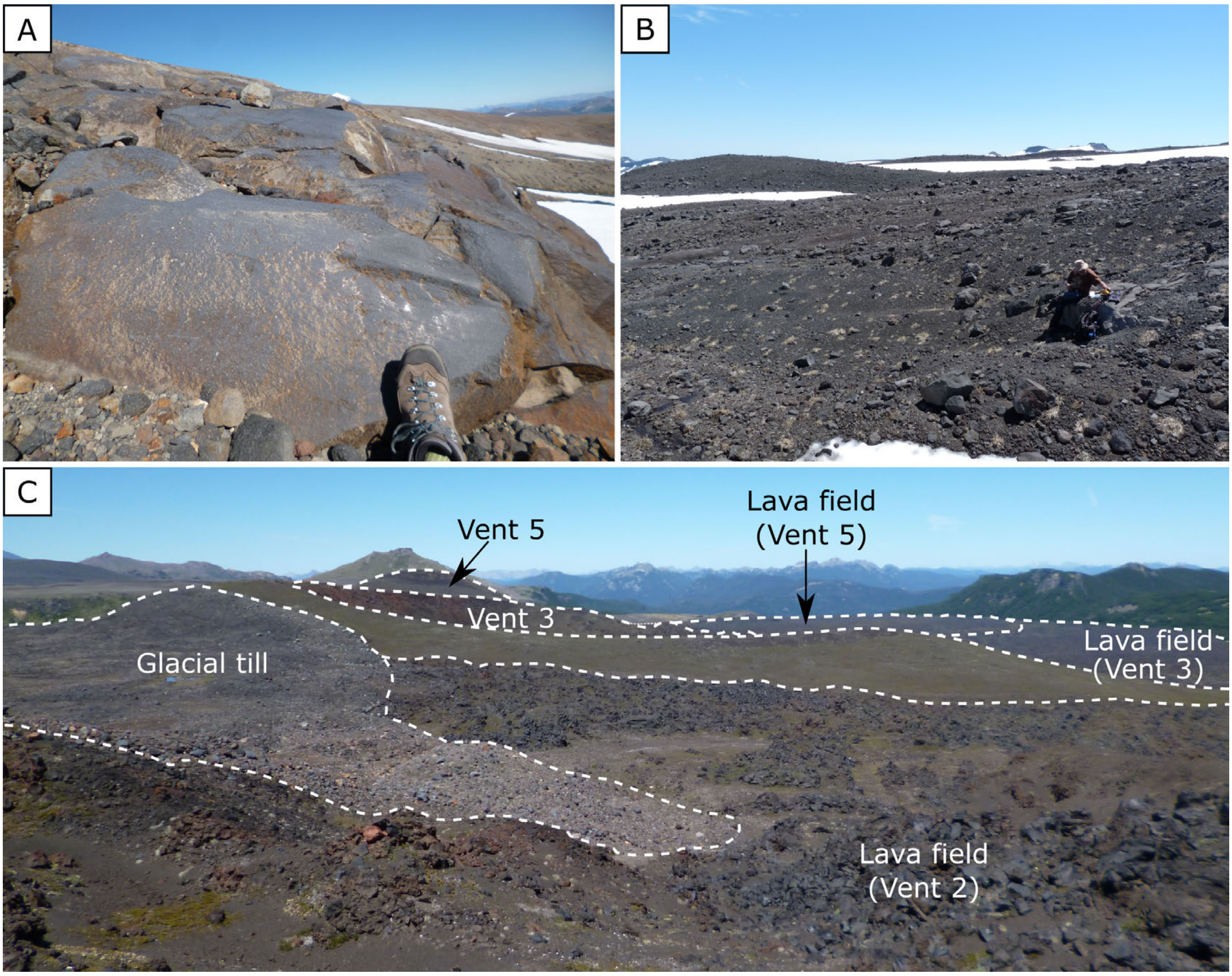

Figure 4: [A] A scoured Holocene lava from the upper flanks. Striations are faintly visible above the boot, striking in a downhill (240°) direction (looking southeast). [B] Diamict, composed of lava boulders of varying size and fine-grained silt, covers most of the upper flanks of Quetrupillán within the scoured zone, obscuring all underlying lava fields (looking west). [C] Glacial till covers the lava field of Vent 2 and the tuff ring of Vent 3 (looking southeast). The field of view is ~200 m wide.

lán. Also, well-preserved subaerial lavas of nominally Holocene age (see above) exposed below the terminus of the scoured zone can be traced upslope into the scoured zone, where they have been scraped and/or covered in diamict. We conclude that as what are clearly Holocene lavas have been eroded within the scoured zone, it must be a Holocene feature.

An important implication of the Holocene glacial erosion of the stratocone is that crucial evidence related to the growth and construction of the stratocone has been removed, such as the locations, numbers, and volumes of stratocone eruptions. Consequently, the total volume of well-preserved Holocene lava (~225×10^6 m^3; see Subsection *4.4.1*) that lies outside of the scoured zone is therefore a minimum estimate.

No Holocene lavas with well-preserved blocky carapaces were found within the scoured zone. This means the most recent lava erupted from the stratocone has been eroded, and thus must be older than the latest ice advance and retreat. In their study of Nevados de Chillán, Dixon et al. [1999] suggest that young small-scale moraines on Nevados de Chillán may have been formed during late Holocene re-advances such as the Little Ice Age (LIA), which ended at the end of the 19th century [Matthews and Briffa 2005]. From radiocarbon dates, dendrochronological data, and pollen analyses, glacial advances throughout South America are known to have occurred from the 15th to late 19th centuries [Clapperton and Sugden 1988]. Patagonian glaciers reached their maximum limits at various stages throughout the 17th, 18th, and 19th centuries [Mercer 1965], and glaciers in the Andes began to recede within the last two decades of the 19th century [Clapperton 1983].

Given evidence of local ice advances across the An-

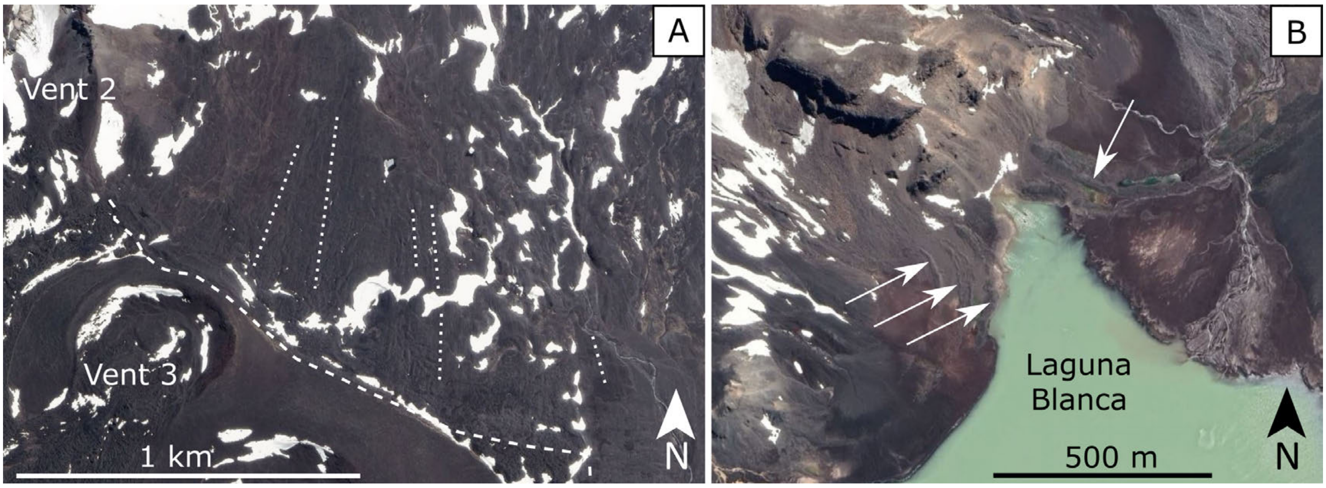

Figure 5: [A] Linear channels are visible in the diamict in satellite images, oriented radially from the summit. The dotted lines highlight some that are visible to the north of Vent 3. The dashed line represents the edge of the moraine. Satellite image from Google Earth (downloaded 09/10/2019). [B] Distinctive curving ridges of glacial deposits are visible in satellite images at the edge of the scoured zone on the shores of Laguna Blanca, highlighted by arrows. Satellite image from Google Earth (downloaded 07/10/2019).

des during the LIA, it is highly likely that glacial advances at Quetrupillán also occurred, with the last one being towards the end of the 19th century. Scouring of the stratocone by ice is likely to have occurred during each period of glacial advance and retreat throughout the LIA. The presence of a clear terminal moraine at the outer limit of the scoured zone, coupled with a lack of terminal moraines within the scoured zone, implies that the most recent glacial advance at Quetrupillán (in the late 19th century) was also the largest and most extensive. As the terminal moraine overlies the youngest erupted lavas on the lower flanks of the stratocone (Figure 4C), this implies that there have been no effusive eruptions within the scoured zone since the major 19th century glacial advance.

The scoured zone of Quetrupillán (2360 m) is unusual, as scrutiny of satellite images suggests that there is no equivalent scoured zone at the nearby volcanoes of either Villarrica or Lanín. Villarrica (2847 m) currently has a much greater ice mass occupying its upper flanks than Quetrupillán, which would have been larger still during the LIA. Although Lanín (3747 m) currently has only a small summit ice cap, its summit lies at a much higher elevation than Quetrupillán, and so during the LIA it is likely that the summit ice mass would have increased and spread substantially.

Temperature fluctuations in the LIA will have resulted in similar and multiple episodes of ice accumulation (in summit regions) followed by ice advance (to lower elevations) at the ice-capped volcanoes of the Villarrica-Quetrupillán-Lanín chain. However, while Quetrupillán was extensively scoured by these LIA ice advances, the same process has not obviously occurred at either Villarrica or Lanín, even though their higher elevations would have led to accumulation of larger ice masses, with the potential to form extensive scoured zones on their stratocone flanks.

The process(es) that formed the scoured zone at Quetrupillán is (are) not known, and require further investigation. It is possible that the location and/or specific glacier-volcano architecture of Quetrupillán resulted in it having a higher sensitivity to LIA conditions, and resulted in the more extensive ice advances and retreats which produced Quetrupillan's well-defined scoured zone, a feature that both Villarrica and Lanín apparently lack.

4.3 Geochemistry and mineralogy

Holocene lavas and eruptive products range in composition from basaltic andesite to trachyte (from 55 wt. % SiO_2 to 66 wt. % SiO_2; Figure 6A; Table 1), with most satellite vents having erupted trachytic magma (64–66 wt. % SiO_2; 7–8 wt. % Na_2O+K_2O). Note that the "T" field on the Total Alkali Silica plot (Figure 6A) includes both trachytes and trachydacites, but following the criteria in Le Maitre et al. [2002] for distinguishing between them, the Quetrupillán rocks in the "T" field are all trachytes. The sampled Holocene lavas erupted from the summit crater also vary in composition from basaltic andesite to trachyte (56–64 wt. % SiO_2).

Trachyte lavas contain phenocrysts and glomerocrysts of pyroxene (augite and enstatite, with minor pigeonite in some samples; Figure 6B), plagioclase (oligoclase to bytownite; Figure 6C), and magnetite and/or ilmenite within glassy groundmass that contains microlites of the same minerals (Figure 7). The trachyandesite and basaltic andesite samples contain phenocrysts and glomerocrysts of pyroxene (augite and enstatite; Figure 6B), plagioclase (andesine to bytownite;

Table 1 – XRF results of samples. Some trace elements were not determined (n.d.) or below detection limit (b.d.l.). Samples were collected from Quetrupillán (Quet), the Trancura Valley (Tran) or the Palguin Valley (Pal).

Location	Vent	Sample type	Sample	Major elements											
				SiO_2	TiO_2	Al_2O_3	Fe_2O_3T	MnO	MgO	CaO	Na_2O	K_2O	P_2O_5	LOI	Total
Quet	1	Lava	Q61	63.92	1.07	15.25	5.42	0.13	1.18	3.18	4.68	2.96	0.33	0.19	98.31
Quet	2	Lava	Q3	64.96	1.11	15.36	5.54	0.13	1.21	3.11	4.85	3.05	0.33	0.20	99.84
Quet	2	Lava	Q53	64.97	1.10	15.63	5.45	0.12	1.18	3.09	4.83	2.96	0.32	0.19	99.84
Quet	3	Lava	Q7	65.03	1.12	15.35	5.56	0.13	1.18	3.12	4.75	3.05	0.32	0.34	99.94
Quet	4	Lava	Q10	64.89	1.11	15.50	5.59	0.13	1.23	3.25	4.77	2.94	0.32	0.03	99.77
Quet	4?	Lava	Q54	64.92	1.08	15.37	5.43	0.13	1.19	3.16	4.90	3.03	0.33	−0.03	99.50
Quet	5	Lava	Q12	64.74	1.15	15.48	5.72	0.13	1.23	3.26	4.83	2.99	0.34	0.11	99.98
Quet	5	Lava	Q56	64.78	1.11	15.36	5.57	0.13	1.20	3.21	4.72	2.96	0.33	0.19	99.55
Quet	6	Lava	Q48	64.24	1.11	15.37	5.59	0.13	1.25	3.30	4.82	2.95	0.35	0.03	99.13
Quet	6	Enclave	Q46	61.56	0.72	16.07	5.97	0.12	3.77	5.49	4.03	2.17	0.17	0.20	100.27
Quet	7	Lava	Q41	64.38	1.10	15.43	5.56	0.13	1.24	3.28	4.74	2.95	0.35	0.03	99.19
Quet	7	Lava	Q43	64.91	1.11	15.46	5.56	0.13	1.18	3.16	4.81	2.97	0.33	0.11	99.71
Quet	8	Lava	Q40	64.49	1.11	15.42	5.52	0.13	1.23	3.25	4.76	2.97	0.35	0.15	99.37
Quet	9	Lava	Q39	65.13	1.08	15.34	5.40	0.12	1.16	3.06	4.82	3.07	0.33	0.03	99.54
Quet	10	Lava	Q50	54.84	1.04	16.23	8.80	0.14	6.50	7.67	3.22	1.48	0.28	−0.21	100.00
Quet	11	Lava	Q8	58.66	1.36	16.17	8.16	0.13	2.89	5.88	3.92	2.34	0.36	−0.02	99.84
Quet	12	Lava	Q17	57.64	1.19	16.51	7.85	0.13	3.63	6.05	3.82	2.20	0.34	0.28	99.63
Quet	13	Lava	Q31	64.52	1.09	15.43	5.59	0.12	1.21	3.15	4.75	3.02	0.29	0.46	99.64
Quet	13	Lava	Q34	64.89	1.08	15.53	5.57	0.13	1.19	3.16	4.82	3.05	0.32	0.22	99.95
Quet	14	Lava	Q29	63.06	1.12	15.46	5.85	0.12	1.35	3.29	4.36	2.77	0.30	1.93	99.63
Quet	14	Lava	Q36	64.05	1.08	15.16	6.61	0.23	1.16	3.06	4.74	3.05	0.31	0.35	99.80
Quet	14	Lava	Q65	64.59	1.05	15.01	5.40	0.12	1.13	2.85	4.66	3.02	0.22	0.41	98.45
Quet	15	Lava	Q69	65.02	1.08	15.22	5.36	0.13	1.14	2.96	4.79	3.07	0.32	0.19	99.28
Quet	Summit	Lava	Q16	55.32	1.07	16.85	8.42	0.14	5.50	7.62	3.17	1.45	0.29	0.08	99.91
Quet	Summit	Lava	Q20	61.06	1.18	16.07	6.77	0.11	2.26	4.62	4.23	2.75	0.35	0.11	99.52
Quet	Summit	Lava	Q23	57.20	1.00	16.65	7.84	0.13	5.14	6.97	3.32	1.80	0.26	0.02	100.34
Quet	Summit	Lava	Q60	58.25	1.17	16.08	7.64	0.13	3.49	5.96	3.80	2.31	0.35	−0.14	99.04
Quet	Summit	Lava	Q62	63.56	1.24	14.97	6.39	0.13	1.39	3.48	4.51	3.16	0.43	−0.06	99.19
Quet	Summit	Lava	Q63	55.37	1.06	16.03	8.01	0.14	5.12	6.94	3.32	1.74	0.28	−0.04	97.96
Tran		Tephra	T1	64.10	1.08	15.70	5.50	0.12	1.09	3.03	4.70	3.02	0.32	1.22	99.88
Tran		Tephra	T2	53.14	1.27	17.76	10.63	0.17	3.44	7.00	3.06	0.73	0.23	2.43	99.86
Tran		Tephra	T5	64.42	1.13	16.01	5.63	0.13	1.21	3.16	4.47	3.02	0.33	0.40	99.91
Tran		Tephra	T6	50.32	1.24	19.16	9.98	0.17	5.76	8.54	2.57	0.88	0.40	0.60	99.62
Tran		Tephra	T7	52.09	1.34	20.37	10.98	0.19	3.37	6.57	2.47	0.67	0.33	1.37	99.75
Tran		Tephra	T8	53.85	1.20	18.17	9.79	0.15	4.06	8.33	2.86	0.75	0.22	0.22	99.60
Tran		Tephra	T9	53.40	1.31	18.75	10.84	0.17	3.65	6.97	2.69	0.73	0.23	1.09	99.83
Tran		Tephra	T10	64.31	1.14	15.84	5.72	0.13	1.53	3.20	4.50	2.86	0.31	0.31	99.86
Tran		Tephra	T12	53.38	1.37	19.58	10.20	0.18	2.72	5.44	2.72	1.20	0.28	2.64	99.71
Tran		Tephra	T13	59.30	1.51	17.46	7.97	0.13	1.56	3.60	3.80	2.63	0.45	1.38	99.79
Tran		Tephra	T14	53.39	1.42	19.46	10.38	0.15	2.74	4.79	2.35	1.18	0.29	3.54	99.71
Tran		Tephra	T15	52.46	1.19	18.20	10.43	0.17	4.74	7.82	2.54	0.68	0.20	1.26	99.69
Tran		Tephra	T16	52.62	1.34	20.32	10.40	0.21	2.72	4.74	2.82	1.08	0.26	3.46	99.96
Pal		Tephra	P13	61.76	0.71	18.75	4.33	0.13	0.80	2.57	4.19	1.67	0.17	4.76	99.85
Pal		Tephra	P17	49.91	0.97	19.77	9.70	0.13	4.81	8.28	2.29	0.44	0.29	3.07	99.66
Pal		Tephra	P21	50.51	0.94	19.43	8.84	0.14	5.88	9.68	2.43	0.54	0.16	1.07	99.63
Pal		Tephra	P23	51.95	1.06	20.86	8.04	0.17	3.16	5.21	2.93	0.82	0.20	5.60	99.98
Pal		Tephra	P24	43.79	1.86	22.32	13.68	0.15	2.66	5.31	1.89	0.27	0.35	7.58	99.85

Continued on next page.

Table 1: [cont.] – XRF results of samples.

Location	Sample	Ba	Th	U	Pb	Nb	Sr	Zr	Y	La	Ce	Nd	Zn	Cu	Ni	Cr	V	Sc	Rb
		Trace elements																	
	Detection limit	3.7	0.4	0.4	0.4	0.1	0.3	0.3	0.2	1.6	2.1	1.4	0.7	0.7	1.0	1.2	2.2	1.0	0.2
Quet	Q61	751.6	n.d	n.d	n.d	14.2	313.3	327.0	43.3	31.4	74.1	41.4	73.2	31.4	2.5	2.6	63.7	15.5	78.6
Quet	Q3	737.8	10.1	2.8	22.7	14.1	284.3	352.2	44.4	32.5	79.2	38.8	71.2	14.5	b.d.l.	4.0	63.7	16.6	77.8
Quet	Q53	710.4	10.3	3.4	21.5	13.3	294.3	337.6	44.5	33.6	81.2	40.9	68.6	13.8	b.d.l.	2.8	63.3	16.0	75.8
Quet	Q7	733.8	10.2	2.7	22.3	13.6	285.5	345.4	43.9	31.7	79.3	38.5	70.3	14.2	b.d.l.	3.0	63.4	17.1	77.1
Quet	Q10	701.8	10.3	3.2	21.8	12.9	292.9	328.0	43.2	32.4	81.2	39.5	70.1	15.3	b.d.l.	3.2	64.8	17.0	74.1
Quet	Q54	754.0	n.d	n.d	n.d	14.5	307.3	331.0	43.6	31.6	74.9	42.2	72.9	15.1	0.5	2.4	64.2	16.2	79.3
Quet	Q12	730.0	10.0	2.6	22.3	13.5	299.6	339.5	43.8	32.3	79.7	38.1	72.5	15.2	b.d.l.	3.5	66.3	17.2	75.4
Quet	Q56	696.4	10.3	3.1	21.8	13.0	296.4	332.7	44.4	34.9	82.7	39.6	69.4	15.2	b.d.l.	3.3	63.0	17.5	n.d
Quet	Q48	744.4	n.d	n.d	n.d	14.2	320.0	322.0	43.4	31.8	74.8	42.5	75.5	15.9	0.2	1.7	70.4	18.1	76.9
Quet	Q46	580.9	n.d	n.d	n.d	8.0	467.5	222.1	28.9	21.1	46.0	24.5	51.5	29.2	30.9	88.1	103.5	15.7	54.5
Quet	Q41	741.0	n.d	n.d	n.d	14.1	320.3	323.9	43.5	30.0	75.0	40.9	71.7	16.5	0.8	1.4	67.6	17.3	77.8
Quet	Q43	697.6	10.3	3.3	21.2	13.2	294.1	337.9	44.4	31.0	81.7	39.7	68.1	13.7	b.d.l.	2.7	62.6	17.8	76.2
Quet	Q40	739.2	n.d	n.d	n.d	14.4	317.0	325.1	43.6	30.9	74.8	40.9	72.2	15.1	0.1	b.d.l.	65.6	16.5	77.8
Quet	Q39	755.3	n.d	n.d	n.d	14.6	299.9	334.7	44.0	30.8	75.4	41.3	70.5	14.1	b.d.l.	b.d.l.	60.6	15.9	80.6
Quet	Q50	402.5	n.d	n.d	n.d	7.4	442.4	177.3	27.8	17.1	41.4	22.6	74.4	56.7	78.3	179.8	210.5	27.3	37.4
Quet	Q8	583.2	8.5	1.6	19.2	10.9	371.8	270.6	36.9	22.5	64.5	32.2	76.1	59.9	18.6	28.2	228.8	24.3	60.3
Quet	Q17	545.1	8.0	2.2	18.6	10.5	389.0	258.1	34.2	23.3	61.1	30.6	73.0	65.5	35.0	78.6	186.1	24.9	56.9
Quet	Q31	731.6	10.4	2.6	23.3	13.6	287.3	346.1	42.3	31.6	77.6	36.3	68.7	18.0	0.4	2.7	70.3	16.4	78.2
Quet	Q34	737.7	10.0	3.2	22.5	13.4	286.2	347.7	43.4	31.4	78.3	38.3	68.3	18.7	b.d.l.	3.5	67.3	16.8	78.4
Quet	Q29	691.8	9.4	2.4	28.9	12.7	288.2	326.0	39.0	29.2	72.4	35.3	72.3	23.1	1.9	9.6	86.0	18.4	70.7
Quet	Q36	736.3	10.1	2.9	21.4	13.7	280.2	349.0	43.5	31.9	78.6	38.3	66.9	13.4	b.d.l.	3.4	67.4	16.0	78.8
Quet	Q65	752.2	n.d	n.d	n.d	14.3	289.6	335.4	40.4	28.3	70.0	36.9	70.8	19.5	0.5	3.2	64.9	15.5	80.4
Quet	Q69	756.7	n.d	n.d	n.d	14.8	294.7	336.6	43.8	31.5	75.5	40.1	70.0	15.0	b.d.l.	2.8	56.9	16.5	80.6
Quet	Q16	403.1	3.8	2.4	10.0	7.1	471.2	166.6	25.8	14.7	45.1	23.7	70.5	51.8	62.5	152.2	191.8	24.8	34.7
Quet	Q20	648.9	9.3	2.8	20.9	12.0	324.6	314.5	39.3	27.5	70.7	35.8	68.6	39.8	12.8	21.2	156.6	19.3	71.4
Quet	Q23	440.9	6.7	2.6	12.9	8.0	410.2	202.4	28.5	19.1	53.0	24.7	64.2	46.5	49.5	141.2	170.9	23.3	45.3
Quet	Q60	581.1	n.d	n.d	n.d	11.3	402.8	260.8	35.6	24.3	57.1	33.4	69.9	46.3	27.8	59.9	172.6	22.4	62.3
Quet	Q62	748.9	n.d	n.d	n.d	15.3	290.9	352.4	47.1	32.1	79.1	44.4	75.9	21.0	1.3	3.1	95.7	18.9	84.7
Quet	Q63	467.7	n.d	n.d	n.d	8.5	416.7	204.1	30.4	19.6	45.2	24.6	68.7	44.1	66.2	154.9	192.8	24.7	45.3
Tran	T1	728.1	10.8	2.8	22.5	13.9	271.1	359.4	44.8	32.5	81.1	40.3	69.9	16.7	b.d.l.	3.8	69.3	16.8	77.1
Tran	T2	237.6	2.4	b.d.l.	9.8	2.9	362.6	115.4	27.5	6.3	24.8	17.4	99.0	108.1	15.2	39.2	332.9	37.8	17.7
Tran	T5	721.8	10.7	3.8	22.7	13.5	274.5	355.3	44.9	34.0	83.9	41.9	68.5	18.3	1.4	2.0	78.1	16.6	73.9
Tran	T6	304.9	2.5	1.6	8.1	7.1	496.4	134.5	23.7	15.2	44.9	22.7	76.9	70.0	65.1	177.7	265.0	36.5	18.2
Tran	T7	262.6	2.2	1.2	9.3	3.6	326.0	109.4	25.8	10.0	34.2	19.8	96.5	97.2	24.6	68.0	297.3	38.2	13.9
Tran	T8	247.7	2.1	1.9	8.2	2.4	413.1	101.9	25.9	6.0	24.6	17.1	97.0	105.7	29.9	53.3	312.7	34.8	17.3
Tran	T9	301.2	1.0	1.6	9.4	2.6	353.6	115.4	28.8	8.7	26.1	17.5	111.0	120.7	28.0	43.9	334.7	37.7	17.2
Tran	T10	695.0	9.8	3.6	22.8	12.8	304.2	329.6	42.4	32.9	75.3	39.0	72.8	12.6	3.4	10.1	70.8	18.4	68.8
Tran	T12	447.4	7.5	2.6	15.8	7.0	410.2	185.4	43.5	27.7	55.0	37.1	92.4	114.3	16.4	55.3	259.3	36.5	25.7
Tran	T13	640.6	12.3	3.4	28.0	14.8	259.2	387.1	47.2	37.6	85.9	46.3	76.0	33.7	4.0	3.7	154.3	24.6	62.8
Tran	T14	423.7	7.6	2.2	19.7	7.3	286.5	212.8	37.1	21.9	57.5	31.6	94.5	82.0	22.6	67.0	283.4	36.6	25.8
Tran	T15	223.5	0.7	1.5	8.6	2.4	345.7	106.9	26.2	6.5	25.7	17.1	94.6	93.7	41.0	94.6	312.7	40.8	15.3
Tran	T16	346.2	5.8	1.6	15.4	6.2	310.3	182.2	40.5	20.8	54.5	33.6	92.4	127.9	27.2	81.2	234.5	37.3	23.2
Pal	P13	735.0	6.1	2.3	18.9	7.0	372.0	244.8	46.1	21.4	60.2	34.0	89.5	10.3	5.3	5.3	44.1	19.1	40.7
Pal	P17	206.6	b.d.l.	1.3	7.7	2.3	410.4	51.8	21.0	3.3	22.3	13.8	66.1	94.2	53.4	150.7	281.1	50.2	9.8
Pal	P21	226.8	3.0	1.9	9.5	1.7	586.2	22.3	18.1	2.8	21.6	13.6	70.1	117.3	81.3	188.3	291.7	41.2	10.9
Pal	P23	354.1	5.1	2.0	17.4	5.0	381.5	116.1	36.8	15.5	46.7	27.6	77.8	101.4	38.4	82.7	201.7	37.8	18.9
Pal	P24	209.6	3.0	1.4	12.2	3.4	411.9	87.3	34.5	8.5	38.0	26.7	63.9	146.8	35.3	68.5	467.8	64.6	5.3

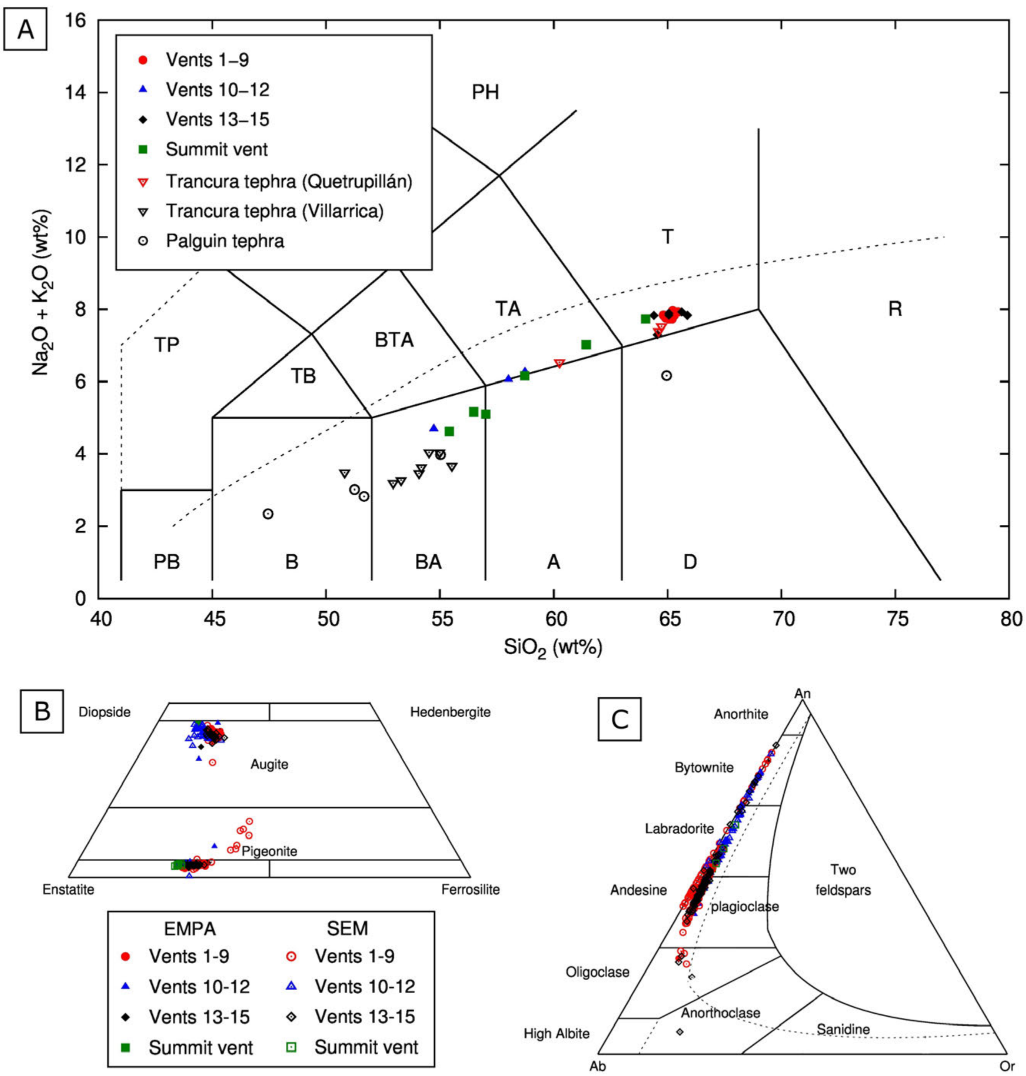

Figure 6: Geochemical diagrams of lavas from Quetrupillán. [A] Total alkali silica plot (including tephra deposits in the Trancura and Palguin Valleys). [B] Pyroxene compositions. [C] Feldspar compositions. Samples are grouped according to their source vent: red circles – Vents 1–9; blue triangles – Vents 10–12; black diamonds – Vents 13–15; green squares – summit vent; inverted red triangle – Quetrupillán Trancura tephra; inverted black triangle – Villarrica Trancura tephra; open black circle – Palguin tephra. In diagrams [B] and [C] filled symbols represent data collected by EMPA and open symbols represent data from the SEM.

Figure 6C), olivine with resorbed rims, and magnetite (Figure 7). Groundmass glass and melt inclusions have compositions that range from basalt to high-silica trachyte and rhyolite. Lavas contain two populations of plagioclase phenocrysts, a pristine euhedral population and a population with resorbed rims, sieve-textured interior, and composition that varies from rim to core.

Tephra deposits preserved in valleys surrounding Quetrupillán were analysed by XRF in order to determine their provenance (Table 1). Trace element abundances were compared with the characteristic elemental abundances from Quetrupillán, Villarrica, and Lanín (Figure 8; this work and other sources, see Supplementary Material for references). Tephra produced by Quetrupillán has compositions of trachyte and trachyandesite (Figure 6A).

4.4 Satellite vents and lavas

The most obvious and best-preserved products of Holocene volcanism at Quetrupillán are the sixteen exposed vents and their associated lavas that lie around the lower flanks of the stratocone (labelled in Figure 2). Twelve of these sixteen vents lie in a volcanic field that is located 3–7 km south of the stratocone summit. In this southern volcanic field, the volumetrically dominant erupted composition is trachyte (Table 2), with just one eruption of basaltic andesite and two eruptions of trachyandesite. The three vents on the eastern flanks of Quetrupillán (Vents 13, 14, and 15) have erupted

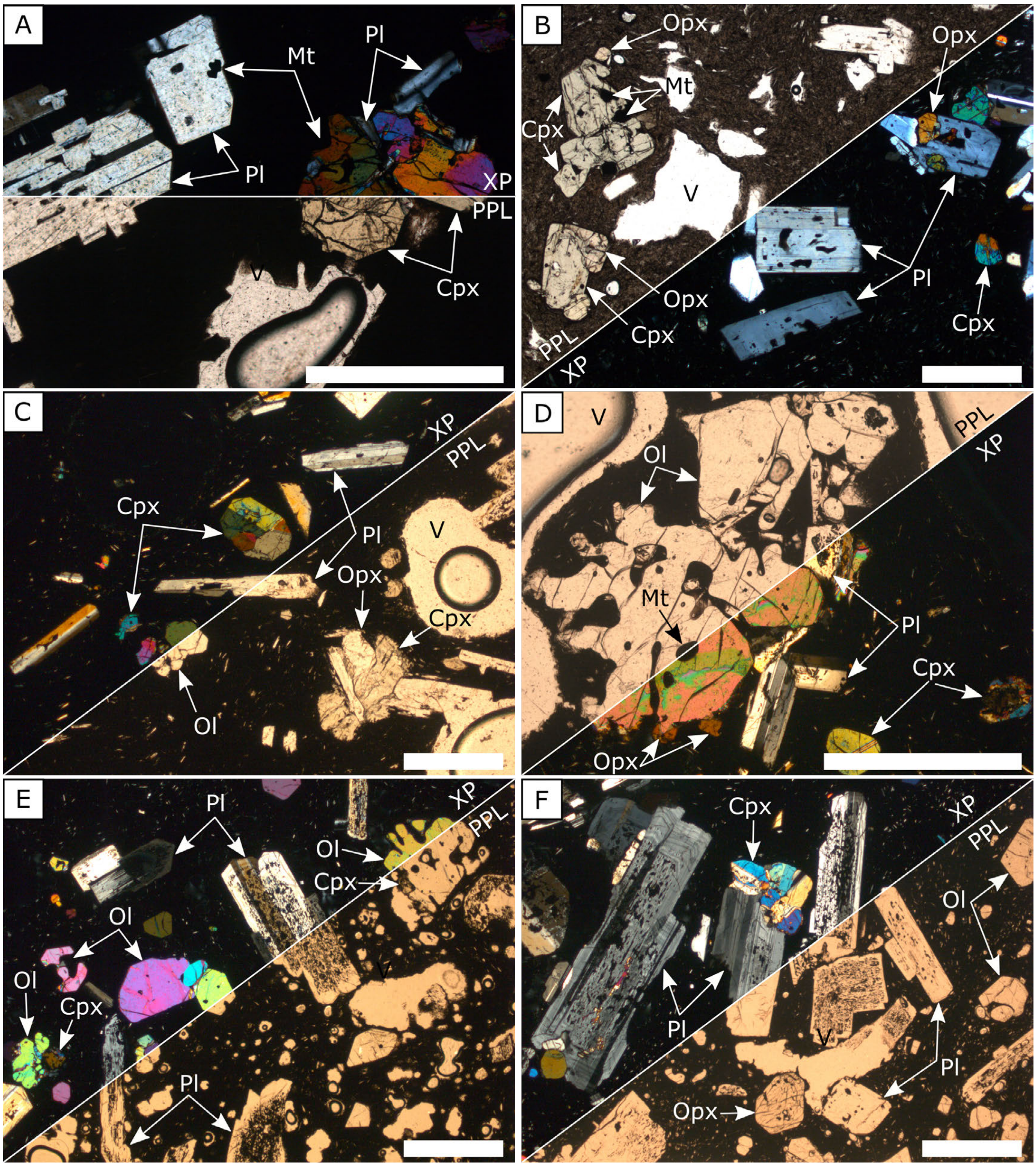

Figure 7: Thin section images of lavas from satellite vents at Quetrupillán, of trachyte ([A] and [B]), trachyandesite ([C] and [D]) and basaltic andesite ([E] and [F]) composition. Pl – plagioclase, Cpx – clinopyroxene, Opx – orthopyroxene, Ol – olivine, Mt – magnetite, V – vesicle. Scale bar in each image is 1 mm. Images show thin sections under plane polarised light (PPL) and under crossed polars (XP).

trachyte and have produced two sizeable scoria cones, along with a number of trachytic lavas that have flowed east until they met a ~250 m high (fault) scarp and were channelled northwards along the Huililco Valley, against the lower edge of the scarp. Vent 16 is evident on aerial imagery but was not visited during fieldwork and so its composition is unknown.

Most of the vents that lie within the southern volcanic field lie along two lineaments. Vents 1 to 5 (labelled in Figure 2) lie along a 2.7 km long lineament

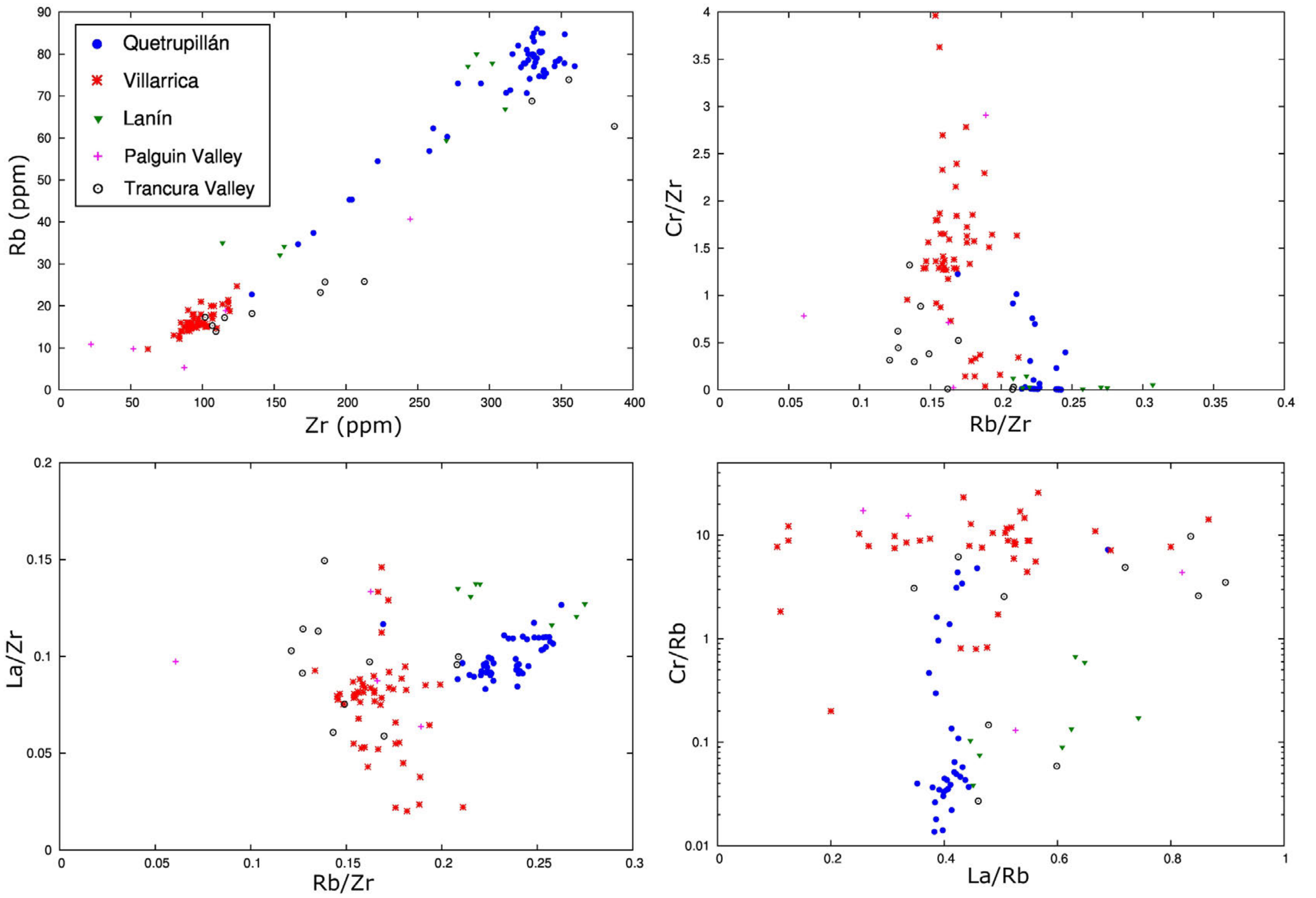

Figure 8: Trace element abundances of tephra samples from the Palguin Valley (pink crosses) and Trancura Valley (open black circles), compared with Quetrupillán (blue circles), Villarrica (red stars) and Lanín (green triangles). Data for Quetrupillán, Villarrica and Lanín is from this work and work by other authors. See Supplementary Material for full references.

orientated at 157°. This is roughly parallel to the Pleistocene trachyte fissure that lies to the west of Laguna Azul [McGarvie 2014], and is approximately perpendicular to the alignment of Vents 7, 8, and 9 (048°). Field evidence indicates that each of the vents within this volcanic field were only active for the duration of the related eruption.

As Holocene volcanism at Quetrupillán has not been the subject of a detailed study, we provide a description of the volcanic features, with a focus on the trachyte lavas.

4.4.1 *Trachyte lavas*

Of the sixteen flank vents at Quetrupillán, thirteen have effused lavas, which range in volume from ~0.9×10^6 m^3 to over 61×10^6 m^3 (Table 2). Of these, ten vents have produced trachyte lavas (over 200×10^6 m^3 in total), while two have produced trachyandesite lavas (4.1×10^6 m^3) and one has produced basaltic andesite lava (3.4×10^6 m^3).

Trachyte lavas on Quetrupillán commonly contain patches of oxidised, red spatter fragments, which increase in abundance towards their source vents (Figure 9A). As such, they are interpreted as clastogenic lava flows, formed when accumulated spatter is sufficiently molten to coalesce and remobilise into a lava flow [Andronico et al. 2008; Sumner 1998]. The trachyte lavas form blocky lava fields, with surfaces, flanks and termini consisting of black, glassy blocks that range in size from <30 cm to 1.5 m (Figure 9B). The blocks have a combination of rough, vesicular, irregular surfaces, and smooth, planar surfaces bounded by straight, sharp edges (Figure 9C and 9D), characteristic of typical blocky lava flows [Cigolini et al. 1984; Macdonald 1953].

Many trachyte lava fields have ogives (arcuate ridges orthogonal to flow direction) on their surface, caused by folding and wrinkling of the lava flow crust during emplacement [Fink 1980; Magnall et al. 2017]. This is most clearly observed in aerial images of the lava field from Vent 5, where well-developed ogives are 40–80 m in wavelength and up to 15 m in amplitude (Figure 10A). Several of the lava fields have rubbly levees along their margins (Figure 10B), forming the edges of what was, during emplacement, the active flow chan-

Table 2 – Composition, areas, and volumes of lava fields produced by satellite vents on the flanks of Quetrupillán.

Vent	Location	Composition	Area (km^2)	Thickness (m)	Volume ($\times 10^6$ m^3)	Notes
1	39°31’40” S, 71°44’09” W	Trachyte	NA	NA	NA	No lava field
2	39°32’12” S, 71°44’01” W	Trachyte	1.07	10	10.7	Includes assumed area below moraine
3	39°32’35” S, 71°43’51” W	Trachyte	6.16	10	61.6	Includes assumed area under Vent 5 field. May extend further south in the forested valley towards the cones of Llizan.
4	39°32’49” S, 71°43’36” W	Trachyte	0.13	10	1.3	Only includes exposed area. It will extend below the fields of Vents 3 and 5.
5	39°32’54” S, 71°43’31” W	Trachyte	2.30	25	57.5	
6	39°33’24” S, 71°42’19” W	Trachyte	0.50	10	5	
7	39°33’49” S, 71°41’17” W	Trachyte	3.06	10	30.6	May extend below Vent 3 field
8	39°33’37” S, 71°41’06” W	Trachyte	NA	NA	NA	No lava field
9	39°33’24” S, 71°40’43” W	Trachyte	0.23	5	1.2	
10	39°33’01” S, 71°41’45” W	Basaltic andesite	0.67	5	3.4	
11	39°32’48” S, 71°41’12” W	Trachyandesite	0.63	5	3.2	
12	39°31’50” S, 71°42’13” W	Trachyandesite	0.18	5	0.9	
13	39°31’06” S, 71°40’09” W	Trachyte	0.88	10	8.8	Not including any of the flow in the forested Huililco Valley
14	39°30’38” S, 71°40’25” W	Trachyte	1.98	10	19.8	Not including any of the flow in the forested Huililco Valley
15	39°29’40” S, 71°41’08” W	Trachyte	2.09	10	20.9	Not including any of the flow in the forested Huililco Valley
16	39°29’05” S, 71°43’30” W	NA	NA	NA	NA	No lava field, vent not visited

nel [Sparks et al. 1976]. The lava field of Vent 5 is the thickest of all Holocene lava flows, with steep flow margins up to 25 m high defined by well-developed levees (Figure 10A). Numerous breakout lobes have also formed along the margins of this lava field (Figure 10A and 10C).

Five channelized lava flows are visible in aerial images of the large (~30 × 10^6 m^3) trachyte lava field from Vent 7, highlighted by ogives on their surfaces and bounded by marginal shear zones (Figure 11A; Tuffen et al. [2013]). During emplacement, separate channels were active at different times as the lava flowed downslope. In contrast, the emplacement of lava from Vent 6 across relatively flat topography may account for the fact that no features of channelisation are visible. Instead, the lava field has expanded laterally across the plain.

4.4.2 *Trachyte Vents*

Seven of the satellite vents have constructed scoria cones (Figure 11B), of which four are trachytic, and of which all but one have produced lava fields. These are interpreted to have been created by conventional Strombolian activity, with magma fragmentation producing tephra, scoria, and bombs which followed bal-

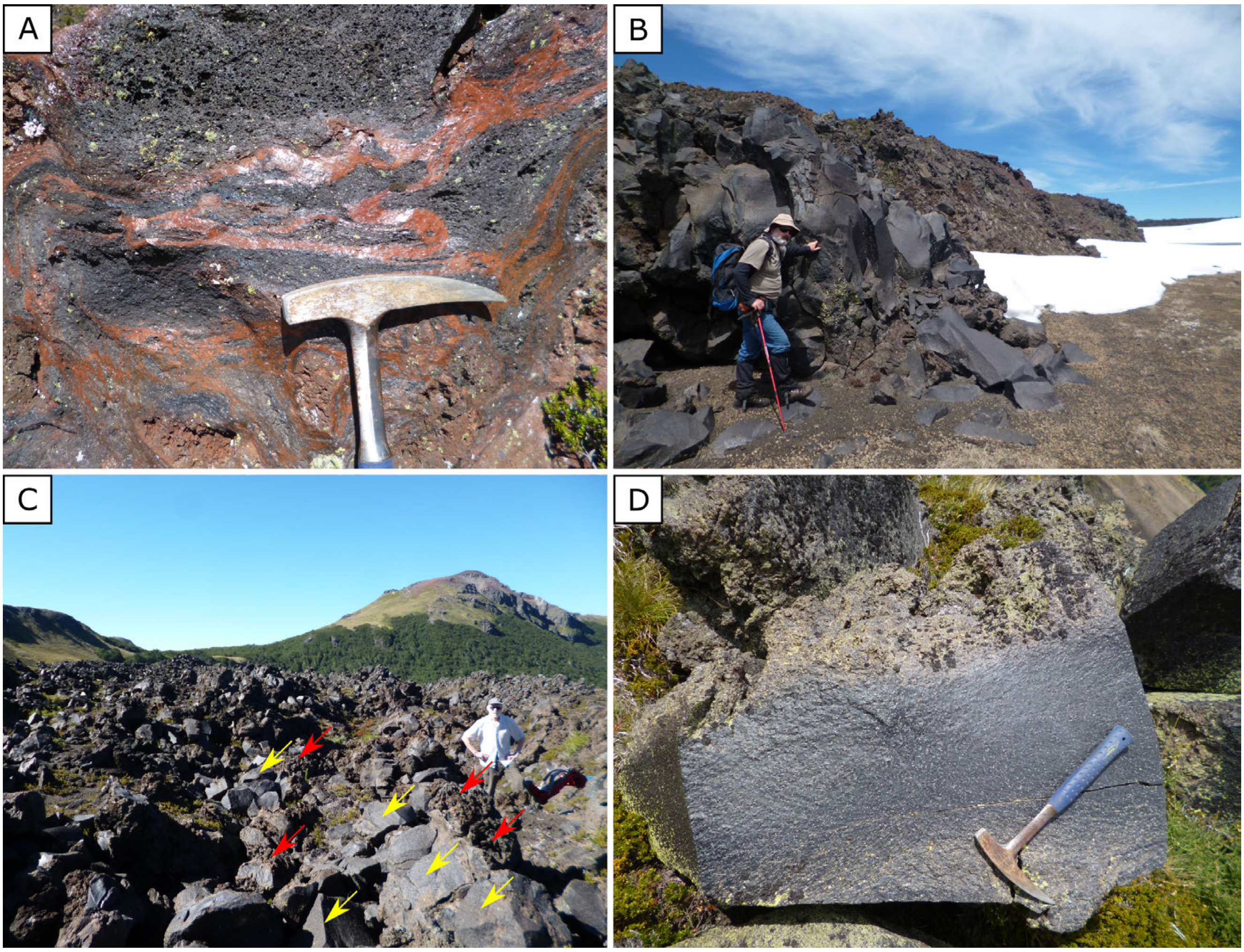

Figure 9: Trachytic blocky lavas. [A] Trachyte lava from Vent 13 that contains red oxidised patches. [B] The steep flow front of the lava field from Vent 7 (looking west), composed of polyhedral blocks of black, glassy trachyte. [C] The lava field from Vent 2 (looking east). Polyhedral blocks have a combination of smooth, planar surfaces with straight sharp edges (yellow arrows) and rough, vesicular, irregular surfaces (red arrows). [D] A lava block from the lava field of Vent 13, showing the contrasting smooth and spinose edges to the polyhedral lava fragments.

listic trajectories to be deposited surrounding the vent [McGetchin et al. 1974; Valentine and Connor 2015]. The scoria cones range in height from 25 m to 120 m and have average basal diameters of ~290 m to 650 m, though all are asymmetric in shape due to a combination of prevailing wind direction, underlying palaeoslope, and conduit orientation [Tibaldi 1995].

There is evidence at some satellite vents that water has been involved in the eruptive activity. Two trachyte vents (1 and 2) have excavated craters through pre-existing volcanic deposits (Figure 11C). Both craters have similar dimensions of ~270 × 400 m, with their long axes aligned with the strike of the associated fissure. A small amount of pyroclastic material has accumulated on the eastern rim of Vent 1, and no lava has been produced. There is an absence of pyroclastic deposits on the crater rim of Vent 2, but lava flows have effused from the vent and flowed southwest and southeast (Figure 1). We interpret that explosive phreatic eruptions formed these craters when rising magma encountered groundwater within the bedrock. Once the groundwater supply had been exhausted (i.e. the water: lava ratio had been greatly reduced), pyroclastic material was erupted at Vent 1 and effusion of lava occurred at Vent 2.

Three trachyte vents (3, 4, and 8) have produced shallow craters with diameters of ~400 m, surrounded by low-rimmed mounds of tephra with gently sloping sides (Figure 12A). The interior walls of the craters are composed of vesicular, welded spatter while unconsolidated tephra (vesicular bombs, lapilli, and ash) drape the outer rims. We interpret these as tuff rings, formed during phreatomagmatic eruptions when interaction between magma and sufficient external water caused explosive fragmentation [Lorenz 1986; Wohletz and Sheridan 1983]. As the influence of groundwa-

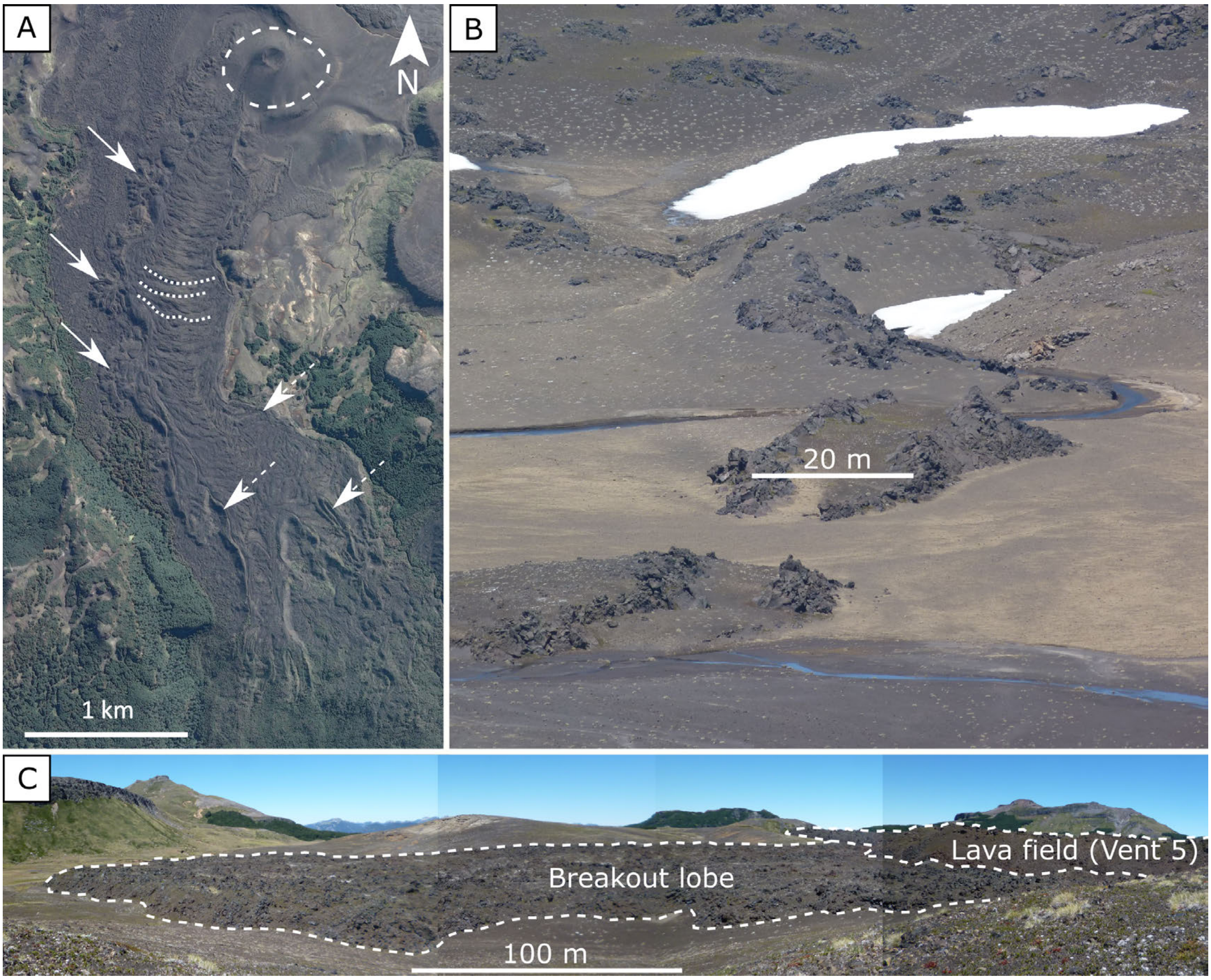

Figure 10: [A] Satellite image of the lava field from Vent 5 highlighting ogives in the flow interior (dotted lines), spidery breakout lobes (solid arrows) and levees along the flow margins (dashed arrows). The dashed line outlines the scoria cone built around Vent 5. Satellite image from Google Earth (downloaded 03/12/2018). [B] Rubbly levees along the edge of a lava field from Vent 11 (looking south from Vent 12). The lava channel is 20 m wide. [C] A breakout lobe from the lava field of Vent 5 (looking south).

ter waned, lava flows effused from Vents 3 and 4 and breached the tuff rings. Spines of lava aligned with the flow direction are interpreted as remnants of the breached tuff ring ramparts that have been transported in the lava flow (Figure 12B). As only three of the satellite vents of Quetrupillán have produced tuff rings, this suggests that the presence of water was both transient and local, given that neighbouring vents active during the same fissure eruption do not show any features indicating magma-water interactions.

The vigour of explosive phases of Holocene eruptions is reflected in the extent and character of tephra blankets that occur generally to the east (i.e. downwind) of vents. For example, a particularly vigorous explosive phase is inferred to have occurred from Vent 11, as a tephra blanket which consists of agglutinated trachyandesite spatter ~10 m thick at a distance of 1 km from the vent (Figure 12C) covers the ridge of Cerro Colorado, southeast of Laguna Blanca (see Figure 2 for location of named places).

4.4.3 *Eruption stratigraphy of the satellite eruptions*

Stratigraphic relationships can determine the relative ages of some of the lava fields from the satellite vents on the flanks of Quetrupillán (Table 3; Figure 2). However, many of the lava fields are geographically isolated and so it is not possible to determine their relative stratigraphy. It was not possible to use tephrostratigraphy to assist with this, as tephra deposits are poorly preserved on the exposed, unvegetated flanks of Quetrupillán and are only locally preserved. In addition, thick snow covers the area during winter months, so any tephra deposited on the snow would be removed or modified

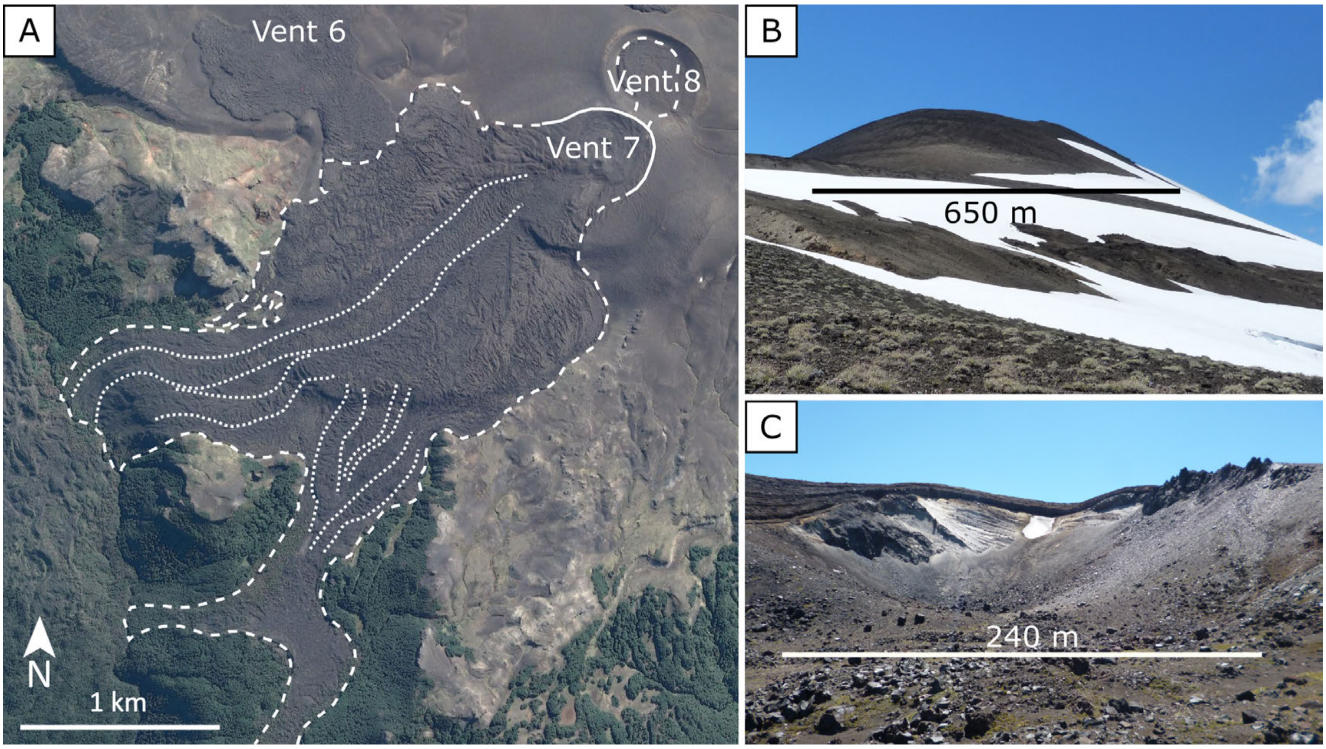

Figure 11: [A] Satellite image of the lava field from Vent 7. Five channelized lava flows are highlighted with dotted lines. Satellite image from Google Earth (downloaded 03/12/2018). [B] The scoria cone of Vent 14 (looking north). The cone has a basal diameter of 650 m. [C] The Pre-Holocene lavas and pyroclastics exposed in the excavated crater of Vent 2 (looking north). The crater width is 240 m.

during melting in spring. For this reason, the stratigraphy presented in Table 3 must be considered as tentative as well as incomplete.

In the southern volcanic field the most recent eruption occurred from a fissure to the east of Laguna Azul, with activity from Vents 1 to 5 (termed Eruption A). The lava field of Vent 4 is overlain by the lava field of Vent 3, which is in turn overlain by the lava field of Vent 5, indicating that activity began at Vent 4. The younger Vent 5 has also constructed a scoria cone on the edge of the older tuff ring formed around Vent 4. The lava field of Vent 2 diverges around and overlies the tuff rings of Vents 3 and 4 and so must be younger than they are. This lava has the freshest appearance of all Holocene lavas, and so is interpreted as the youngest lava field of Quetrupillán. Vent 1 did not produce a lava field, and so the relative timing of its activity is unknown.

A second fissure eruption occurred on the southeast flanks of Quetrupillán, with activity from Vents 7 to 9 (Eruption B). The creation of the Vent 8 tuff ring predates the effusion of lava from Vent 7, as lava spills over the tuff ring into the Vent 8 crater. The Vent 7 lava field also spills into the valley containing the Vent 3 lava field, which it underlies, indicating that Eruption B is older than Eruption A.

Vents 6 (Eruption C) and 10 (Eruption D) are located on a plateau of Pre-Holocene lava. The Vent 7 lava field infills the lobate edge of the Vent 6 lava field, indicating that fissure Eruption B is younger than Eruption C. An eroded lobe of lava from Vent 6 overlies the Vent 10 lava field, implying Eruption D pre-dates Eruption C. The Vent 10 basaltic andesite lava field is completely infilled by tephra, with highly weathered lava only occasionally exposed at the edges of the field. This appearance suggests that Eruption D is significantly older than the trachytic Eruptions A, B, and C.

The trachyandesite lava fields of Vents 11 and 12 are geographically isolated, with the lack of contact between them preventing determination of their relative stratigraphy. They have been termed Eruption E and F, respectively (Table 3). On the eastern flanks of Quetrupillán, the Vent 13 lava field (Eruption G) overlies the Vent 14 lava field (Eruption H), indicating that it is younger. The Vent 15 lava field (Eruption I) is geographically isolated, as is the cone of Vent 16 (Eruption J), and so the relative timing of these eruptions cannot be constrained.

4.4.4 *The stratocone*

In Subsection 4.2 we highlighted how the record of Holocene volcanic activity that constructed the stratocone has been removed by repeated ice advances and retreats during the Little Ice Age of the 17th–19th centuries, and evidence suggests that the most recent (19th century) ice advance was also the most extensive. Consequently, a major gap in our understanding of the

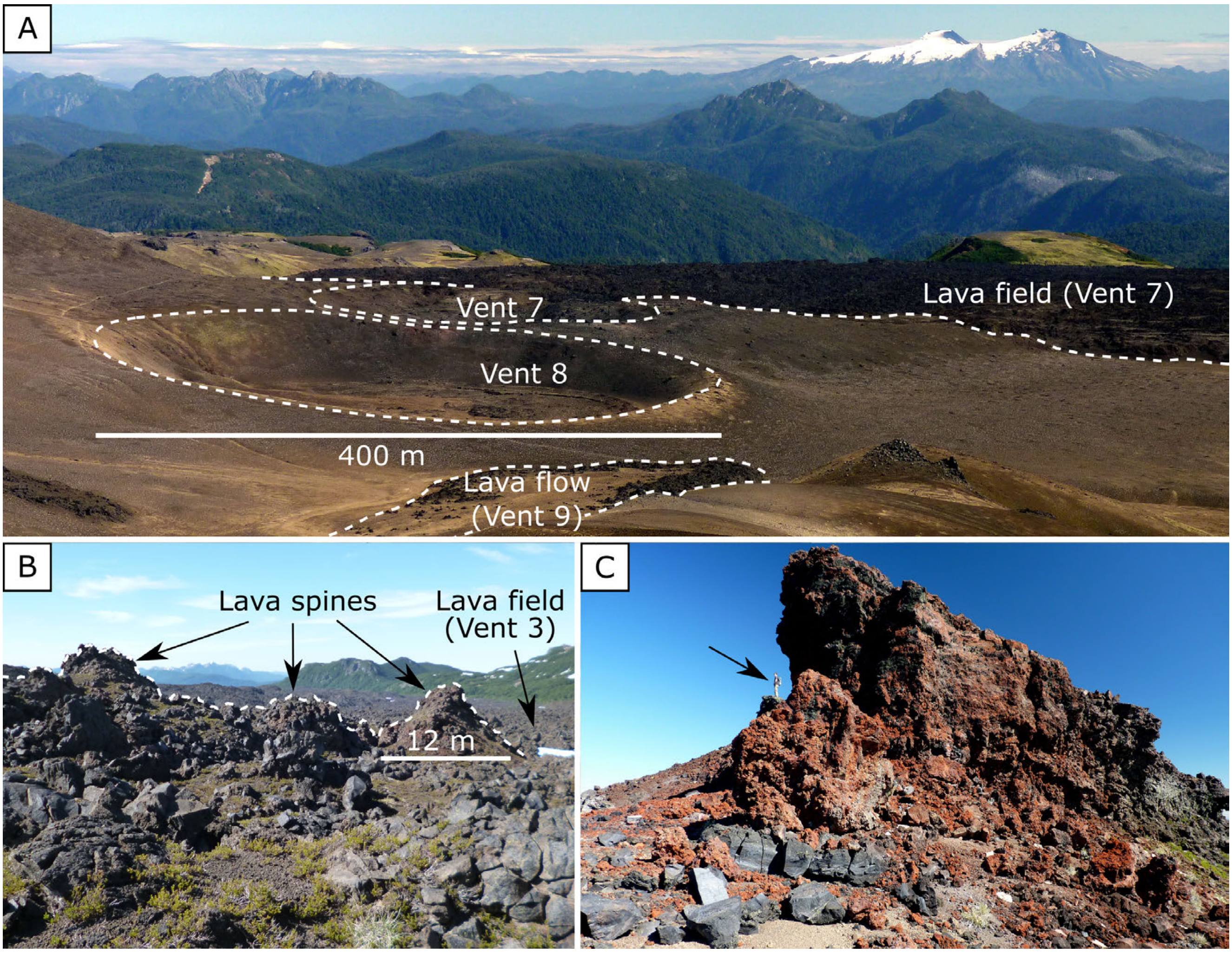

Figure 12: [A] Vent 8 has produced a shallow c.400 m wide crater surrounded by a low-rimmed tuff ring. The lava flow of Vent 9 is visible in the foreground, and Volcán Mocho-Choshuenco is in the background (looking southwest). [B] Lava spines aligned with the flow direction of the lava field of Vent 3 (looking south). [C] A ~10 m thick drape of agglutinated spatter on the ridge of Cerro Colorado. Person for scale, highlighted by arrow (looking NNW).

Holocene eruptive activity of Quetrupillán will be the number, composition and volume of effusive eruptions that took place anywhere on the stratocone. This includes lavas effused from the summit crater and from any satellite vents on the upper flanks of the stratocone within the scoured zone.

The remnants of columnar-jointed trachyte lava buttresses that are exposed within the scoured zone provide evidence that effusion of trachyte lavas from the stratocone took place during the last (Llanquihue) glacial period and/or earlier glacial periods. During past glaciations, relatively thick ice covered the stratocone and surrounding area [Hulton et al. 2002; McGarvie 2014], and so construction of at least an embryonic stratocone must have taken place prior to the Holocene. Logically, construction of the stratocone would have continued during the Holocene, and the partial burial of suspected Llanquihue glaciovolcanic lava buttresses by scoured Holocene lavas supports this.

Within the inner walls of the summit crater are beds of spatter and scoria (mostly oxidised), which are assumed to represent the remnants of an unknown number of eruptions from the summit, of unknown age. Due to accessibility difficulties these were not sampled. Consequently, due to the removal of an unknown amount of lava from the stratocone by Holocene glacial erosion up until the end of the 19th century, it is not possible to state anything definitive about the Holocene construction of the stratocone by lava effusions from either the summit crater or from flank vents within the scoured zone.

4.5 Tephra layers in nearby valleys

Tephra layers are exposed in road cuttings in valleys surrounding Quetrupillán. Two road cuttings were

Table 3 – Relative eruption stratigraphy of activity from the satellite vents.

Eruption	Vents	Stratigraphic evidence	Notes
A	1, 2, 3, 4, 5	Lavas overlie lava from Vent 7 so are younger than Eruption B	This eruptive activity pre-dates the most recent ice advance as the moraine partly covers the lava field of Vent 2 and the tuff rings of Vents 3 and 4 (Figure 4C)
B	7, 8, 9	Lava from Vent 7 underlies lava from Vent 3 so is older than Eruption A. Lava from Vent 7 abuts against the Vent 6 lava field suggesting it is younger than Eruption C	
C	6	The edge of the Vent 6 lava field has an irregular shape which is infilled by the lava field from Vent 7	
D	10	An eroded lobe of lava from Vent 6 overlies the lava field of Vent 10	Lava field is completely infilled by tephra with only small patches of lava exposed
E	11	None – isolated lava field	
F	12	None – isolated lava field	
G	13	Overlies the lava field of Vent 14	
H	14	Underlies the lava field of Vent 13	
I	15	None – isolated lava field	
J	16	None – isolated scoria cone, no lava field	

logged in the Trancura valley near Puesco, to the east of Quetrupillán (Figure 13). An outcrop of Cretaceous granite basement rock is exposed at the base of section T1, presumably cleared of all overlying material during the last glacial period, indicating that the overlying pyroclastic sequence has all been deposited during the Holocene. Eleven tephra layers were identified within this section (Figure 13) of which, according to analysis of trace element abundances (Figure 8), three were produced by Quetrupillán. Villarrica is the source of the remaining eight tephra layers.

Quetrupillán has produced the uppermost two tephra layers in the sequence (Figure 13). The top tephra layer is a 30 cm thick horizon of gritty, grey ash, with abundant modern organic material due to the presence of root matter from the overlying vegetation. It has a trachytic composition (Figure 6A). Below this is a 1 m thick tephra layer which consists of pale, poorly sorted subangular pumice that ranges from 2–40 mm and is interspersed with sparse obsidian lithics. This tephra layer, described elsewhere along the Trancura Valley, is an airfall deposit that has been named the Puesco Pumice by previous studies and dated at 1650 ± 70 yr BP [Toloza 2015] and 1850–1987 cal BP [Fontijn et al. 2016]. Our XRF analysis shows that the Puesco Pumice is trachytic (Figure 9A), and has a similar composition to the Holocene trachyte lava fields on the flanks of Quetrupillán.

The third tephra layer produced by Quetrupillán is in the lower half of the sequence. It is a 15 cm thick horizon of moderately sorted, orange-brown pumice ranging from 1–15 mm with an ashy matrix. This pumice is a trachyandesite (Figure 6A).

At the two locations in the Trancura Valley that were logged and sampled for this paper, all three of the Quetrupillán tephra layers had the characteristics of airfall deposits. There was no clear evidence of characteristics representing the lateral movement of clasts that characterise pyroclastic density current deposits.

A pyroclastic sequence in the Palguin Valley to the northwest of Quetrupillán was also studied. Analysis of trace element abundances (Figure 8) suggests that none of the sampled tephra layers were produced by Quetrupillán.

5 Discussion

5.1 The pattern of Holocene volcanism

The clearest expressions of Holocene volcanism at Quetrupillán are the satellite vents and their lavas. Compositionally, these are trachytes, trachyandesites, and basaltic andesites, with trachytes being volumetrically dominant (Table 2; Figure 6A). Limited analyses

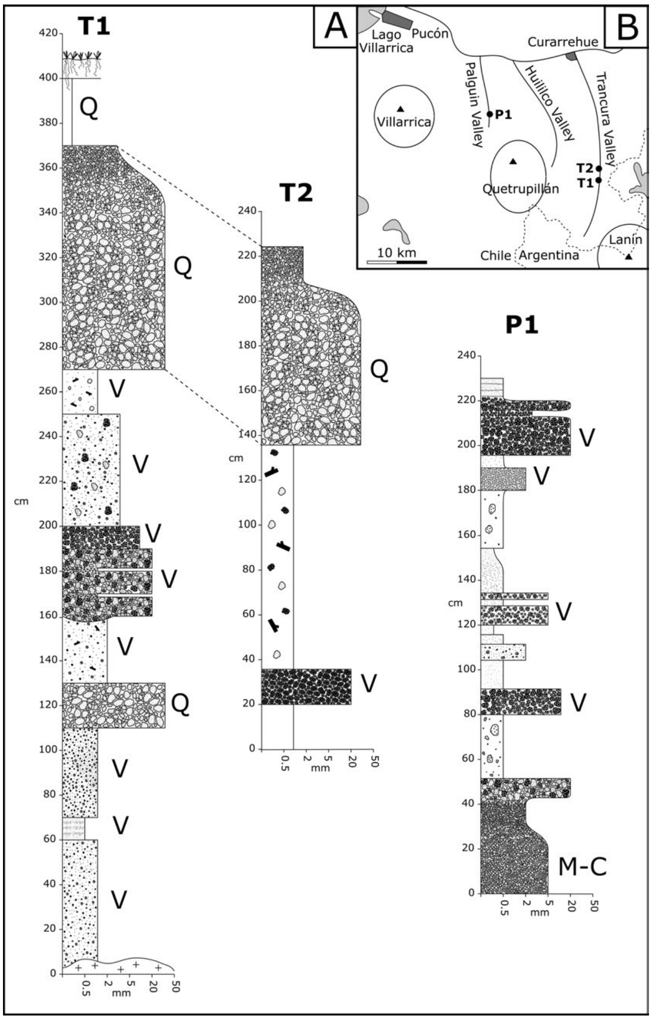

Figure 13: [A] Logs of three pyroclastic sequences studied and sampled in the Trancura Valley (T1 and T2) and the Palguin Valley (P1), with labels identifying tephra layers from Quetrupillán (Q), Villarrica (V) and Mocho-Choshuenco (M-C). [B] Schematic map showing the location of the logged sections in relation to Quetrupillán. T1: 39.52365°S, 71.55047°W; T2: 39.51823°S, 71.54813°W; P1: 39.42695°S, 71.76594°W

of lavas from the eroded stratocone indicate eruption of the same compositional range from the summit region. Consequently, there is no spatial-compositional pattern at Quetrupillán, as seen at some volcanic complexes, as all three magma types have been erupted both at the stratocone and from the satellite vents. In contrast, at Nevados de Chillán, the Cerro Blanco subcomplex erupts basaltic andesite and the Las Termas subcomplex erupts dacite to rhyolite [Dixon et al. 1999; Mee et al. 2009]. This suggests that the plumbing system beneath Quetrupillán is in a less-ordered state.

There is a noticeable "non-eruptive" arc of ~8 km in length around the western and northern margins of the scoured zone, in which there is only one vent (Vent 16; Figure 2), that appears to have produced only a small scoria cone. Elsewhere, gaps between vents are from a few hundred metres up to 2 km, with a concentration of twelve of the sixteen satellite vents in a ~6 km long sector to the south of the stratocone, that we have termed the southern volcanic field. This pattern may be related to a tendency for crustal rupturing to be focused in a zone south of the stratocone, associated with fault splays from the nearby Liquiñe-Ofqui Fault Zone [e.g. Cembrano and Lara 2009; Schonwalder-Angel et al. 2018]. It is notable that Vents 1–5 lie on a distinct fissure, as do Vents 7–9. Further evidence of crustal rupturing in this zone comes from two NNE-striking Pleistocene subglacial trachyte fissure eruptions that flank Laguna Azul [McGarvie 2014].

It is not possible to determine how many eruptions have occurred from the summit of the stratocone, as glacial scouring has removed evidence of Holocene lava stratigraphy. However, as presented in Subsection 4.4.4, within the scoured zone are numerous eroded Holocene lava fields that have flowed around suspected Llanquihue-age lava buttresses, and have partly buried them. From this, we suggest that the stratocone grew during the Holocene as a result of substantial pre-LIA lava effusions that resurfaced its upper flanks. However, the lack of pristine lavas within the scoured zone implies there have been no lava effusions on the upper flanks of the stratocone since the end of the LIA in the late 19th century.

To evaluate the number of Holocene eruptions from the satellite vents, we consider two contrasting scenarios; a simple scenario (i.e. fewest eruptions), and a complex scenario (i.e. the maximum reasonable number of eruptions). In the most complex scenario, each identified vent represents a separate eruptive episode. This would imply that sixteen eruptions have occurred on the lower flanks of Quetrupillán. An argument against this is that the orientation and physical nature of Vents 1–5 indicate that they lie along a fissure, and so would have all been active during the same eruptive episode.

The simple scenario involves just three eruptions: one trachyte eruption, one trachyandesite eruption, and one basaltic andesite eruption. If all the trachyte vents were produced during just one eruption, then this eruption occurred along an arc of ~14 km in length, from Vent 1 in the west to Vent 15 in the northeast (possibly longer if Vent 16 is trachyte; Figure 2). This single trachyte eruption would define an arc that may be related either to a previous ring fracture (caldera fault), or to a more recent crustal weakness that could be activated during a future caldera-forming eruption.

We currently favour an intermediate scenario, whereby the sixteen vents represent ~10 different eruptive episodes, as presented in Table 3. Vents 1–5 and Vents 7–9 represent fissure eruptions, with several vents active during a single eruptive episode, as discussed in Subsection 4.4.3. The remaining vents are likely to represent individual eruptions.

5.2 Hazard implications

This study provides additional information on the potential hazards from effusive and explosive eruptions that complements the existing "Mapa Preliminar De Peligros Del Volcán Quetrupillán" (Preliminary Hazard Map of Quetrupillán Volcano) published by the Servicio Nacional de Geología y Minería [SERNAGEOMIN 2013]. Our study contributes no new information on lahar hazards as we did not find any conclusive evidence of preserved lahar deposits.

5.2.1 *Effusive eruptions*

Holocene lavas (largely trachytes) from the stratocone and satellite vents have flowed down valleys and travelled a maximum of ~15 km from their source vents. Lavas are channelled to the north along the Huililco Valley towards Catripulli, a lava pathway of ~17 km from Quetrupillán's summit, or to the south, where it is a ~30 km lava pathway from the summit to Liquiñe (see Figure 1 for named settlements). To the west there is a potential lava pathway of ~22 km from the summit towards Coñaripe, but there are no known Holocene lavas that have travelled in this direction.

Provided future eruptions occur in the vicinity of known Holocene vents, there is little possibility of lavas causing damage to any larger settlements. Given the distances involved and the expected relatively low velocities of trachytic lavas, and assuming good communication, there should be ample time for evacuation of remote properties located in the higher valleys surrounding Quetrupillán.

5.2.2 *Explosive eruptions*

During this study, three pyroclastic sequences were logged and sampled to evaluate explosive eruptive activity from Quetrupillán (Figure 13). One section was to the northwest, in the Palguin Valley, and two sections were to the east, in the Trancura Valley. The prevailing wind is towards the east, so it was anticipated that the Trancura section would provide the most comprehensive record of explosive volcanism from Quetrupillán. The Palguin section was chosen as it was likely to contain tephra only from the largest of Quetrupillán's explosive eruptions, as it is orthogonal to the expected west-to-east dispersal axis of Quetrupillán eruptive plumes [SERNAGEOMIN 2013].

Trace element analyses of tephra layers in the Palguin Valley indicate that none of the sampled tephra layers have been produced by Quetrupillán (Figure 8). Instead, one dacite layer comes from Mocho-Choshuenco [Rawson et al. 2015], and the rest are from Villarrica, which lies 15 km to the west (upwind). The absence of any tephra from Quetrupillán suggests that there have been no very large explosive eruptions from Quetrupillán in the Holocene.

In the Trancura Valley, trace element analyses identified three tephra layers from explosive eruptions at Quetrupillán (Figure 8), of which two are trachytic and one is trachyandesite (Figure 6A). This section is notable as it covers the entire Holocene, with the lowermost tephra sitting directly on the plutonic basement (Figure 13).

According to information provided by Servicio Nacional de Geología y Minería [SERNAGEOMIN 2019], which appears to be based on the undergraduate dissertation study by Toloza [2015], nine explosive eruptions from Quetrupillán are preserved in the Trancura Valley. Our findings disagree with this, as we only assign three units to Quetrupillán, and consequently the hazard from explosive eruptions affecting areas to the east (e.g. the Trancura Valley) is a factor of three less than currently stated by SERNAGEOMIN.

It should be noted that Toloza [2015] does not provide any geochemical evidence to support the claim that there are nine Holocene explosive eruptions from Quetrupillán preserved in the Trancura Valley. Their underlying assumption is that the vast majority of tephra layers in the Trancura Valley must have come from Quetrupillán. However, only by geochemically analysing each unit can the provenance of each tephra layer be established.

Toloza [2015] and the official hazard map [SERNAGEOMIN 2013] also suggest that there is a substantial pyroclastic density current (PDC) hazard from Quetrupillán in the Trancura Valley. Our observations suggest that all three Quetrupillán tephra layers are airfall deposits. We found no evidence of sedimentary structures reflecting lateral transport, characteristic of PDC deposits, nor did any of these three layers show the very poor sorting that characterises PDCs. However, it is notable that Fontijn et al. [2014] and Rawson et al. [2015], who carried out detailed logging and sampling of tephra layers from numerous sites in this region of Chile, both comment on the variability in preservation of tephra even over short distances (i.e. 10s of metres). So whilst we found no evidence of PDC deposition at our two sites, this may exist elsewhere.

In this context, it is important to note that the eroded remnants of the Colmillo del Diablo volcano lie to the east of Quetrupillán, as does the 200–380 m high near-vertical fault scarp along the eastern edge of the Huililco Valley. These form a major topographic barrier that would hinder, if not block, the passage of PDCs moving eastwards from Quetrupillán and into the Trancura Valley. However, should PDCs be channelled northwards down the Huililco Valley by this topographic barrier then they may reach the isolated settlements located there.

In summary, our work suggests that the hazard from explosive eruptions at Quetrupillán is less than the current hazard map indicates [SERNAGEOMIN 2013], given that our geochemical analyses identified only three, rather than nine, units produced by explosive eruptions that have reached the Trancura Valley. We also found no unequivocal evidence of PDC activity at our studied sites in the Trancura Valley. This implies either that no substantial PDCs have been produced during the Holocene, or that the topographic barrier to the east of Quetrupillán has prevented them from reaching the Trancura Valley. However, we wish to emphasise that our studied sections may have occurred away from PDC pathways, and therefore a future target for hazard evaluation would be a detailed study along the length of the Trancura Valley to establish the past pathways of PDCs, should they exist.

6 Conclusions

This paper provides the first detailed account of Holocene volcanism at Quetrupillán. Holocene eruptions have occurred both at the stratocone and from satellite vents on its flanks. The number and type of eruptions from the summit is unknown due to removal of lavas by ice during LIA glacial advances, resulting in the prominent scoured zone. However, glaciovolcanic buttresses on the flanks of the stratocone that are partly buried by scoured summit lavas indicate that some construction has taken place. We suggest that effusive activity from the stratocone summit has been higher during the Holocene than its scoured appearance implies.

We identified sixteen satellite vents on the flanks of Quetrupillán, which we consider to represent ten Holocene eruptive episodes. Satellite vents have produced tuff rings, scoria cones and phreatic craters, as well as extensive lava fields. Some eruptions have occurred on fissures, suggesting that fault splays related to the LOFZ continue to influence the locations of eruptions at Quetrupillán. The volumetrically dominant composition erupted from the satellite vents is trachyte, with minor trachyandesite and basaltic andesite. Limited sampling of stratocone lavas indicates that all three compositions have also erupted from the summit. Thus, unlike some Chilean volcanic complexes, there is no relationship between eruption location and magma composition at Quetrupillán.

Geochemical evidence from tephra layers in the nearby Trancura Valley (downwind of Quetrupillán) indicates that three sizeable explosive eruptions have occurred from Quetrupillán during the Holocene. This is much fewer than the nine eruptions stated by previous workers, however their study provided no geochemical evidence to identify which volcano had produced the deposits. They also state that all deposits were produced by PDC activity, while our examination of tephra layers in road cuttings did not reveal any unequivocal evidence of the lateral transport structures that are characteristic of PDCs. We consider it important to note that there is a substantial topographic barrier that would either hinder or block passage of PDCs from Quetrupillán to the Trancura Valley. We would suggest that a detailed study of multiple road cuttings is undertaken to resolve the issue of PDC activity.

Acknowledgements

The work in this paper forms part of a NERC-funded PhD studentship by Isla Simmons (Grant number NE/L002558/1). Joaquín Cortés received funding from Edge Hill University (RIF grant 1CORTE18) and Santander Universities supported Dave McGarvie. Huge thanks to John Simmons, Franco Vera Rivadeneira, Jack McGarvie and Jonathan Moles for being wonderful field assistants, and to Christa Bönninghoff, Cristian Silva and Claudia Guzmán Roa for help with logistics in the field. We thank Nic Odling, Nicola Cayzer, John Craven, Chris Hayward and Mike Hall at the University of Edinburgh for help with analysis. And finally, thank you the two reviewers for their comments and suggestions which have improved this manuscript, and to Nick Varley and Jamie Farquharson for editorial handling.

Author contributions

Isla Simmons, Joaquín Cortés and Dave McGarvie conducted fieldwork at Quetrupillán, based on initial reconnaissance mapping by Andrés Pavez. Isla Simmons performed subsequent analyses at the University of Edinburgh. Isla Simmons and Dave McGarvie wrote the manuscript, with assistance from Joaquín Cortés. Eliza Calder, Joaquín Cortés and Dave McGarvie assisted with project supervision.

Data availability

The Supplementary Material spreadsheet includes XRF analyses (collected during this study, and data used in this study collected by other authors), mineral analyses and sample locations.

Copyright notice

References

Andronico, D., A. Cristaldi, and S. Scollo (2008). "The 4–5 September 2007 lava fountain at South-East Crater of Mt Etna, Italy". *Journal of Volcanology and Geothermal Research* 173.3-4, pp. 325–328. doi: 10.1016/j.jvolgeores.2008.02.004.

Brahm, R., M. A. Parada, E. Morgado, C. Contreras, and L. E. McGee (2018). "Origin of Holocene trachyte lavas of the Quetrupillán volcanic complex, Chile: Examples of residual melts in a rejuvenated crystalline mush reservoir". *Journal of Volcanology and*

Geothermal Research 357, pp. 163–176. doi: 10.1016/j.jvolgeores.2018.04.020.

Cembrano, J., F. Hervé, and A. Lavenu (1996). "The Liquiñe Ofqui fault zone: a long-lived intra-arc fault system in southern Chile". *Tectonophysics* 259.1-3, pp. 55–66. doi: 10.1016/0040-1951(95)00066-6.

Cembrano, J. and L. Lara (2009). "The link between volcanism and tectonics in the southern volcanic zone of the Chilean Andes: A review". *Tectonophysics* 471.1-2, pp. 96–113. doi: 10.1016/j.tecto.2009.02.038.

Cigolini, C., A. Borgia, and L. Casertano (1984). "Intracrater activity, aa-block lava, viscosity and flow dynamics: Arenal Volcano, Costa Rica". *Journal of Volcanology and Geothermal Research* 20.1-2, pp. 155–176. doi: 10.1016/0377-0273(84)90072-6.

Clapperton, C. (1983). "The glaciation of the Andes". *Quaternary Science Reviews* 2.2-3, pp. 83–155. doi: 10.1016/0277-3791(83)90005-7.

Clapperton, C. and D. Sugden (1988). "Holocene glacier fluctuations in South America and Antarctica". *Quaternary Science Reviews* 7.2, pp. 185–198. doi: 10.1016/0277-3791(88)90005-4.

Denton, G., C. J. Heusser, T. Lowel, P. Moreno, B. Andersen, L. E. Heusser, C. Schluhter, and D. Marchant (1999). "Interhemispheric Linkage of Paleoclimate During the Last Glaciation". *Geografiska Annaler, Series A: Physical Geography* 81.2, pp. 107–153. doi: 10.1111/j.0435-3676.1999.00055.x.

Dixon, H. J., M. D. Murphy, S. J. Sparks, R. Chávez, J. A. Naranjo, P. N. Dunkley, S. R. Young, J. S. Gilbert, and M. R. Pringle (1999). "The geology of Nevados de Chillán volcano, Chile". *Revista geológica de Chile* 26.2. doi: 10.4067/s0716-02081999000200006.

Fink, J. (1980). "Surface folding and viscosity of rhyolite flows". *Geology* 8.5, p. 250. doi: 10.1130/0091-7613(1980)8<250:sfavor>2.0.co;2.

Fontijn, K., S. M. Lachowycz, H. Rawson, D. M. Pyle, T. A. Mather, J. A. Naranjo, and H. Moreno Roa (2014). "Late Quaternary tephrostratigraphy of southern Chile and Argentina". *Quaternary Science Reviews* 89, pp. 70–84. doi: 10.1016/j.quascirev.2014.02.007.

Fontijn, K., H. Rawson, M. V. Daele, J. Moernaut, A. M. Abarzúa, K. Heirman, S. Bertrand, D. M. Pyle, T. A. Mather, M. D. Batist, J.-A. Naranjo, and H. Moreno Roa (2016). "Synchronisation of sedimentary records using tephra: A postglacial tephrochronological model for the Chilean Lake District". *Quaternary Science Reviews* 137, pp. 234–254. doi: 10.1016/j.quascirev.2016.02.015.

Glasser, N. F., K. N. Jansson, S. Harrison, and J. Kleman (2008). "The glacial geomorphology and Pleistocene history of South America between 38°S and 56°S". *Quaternary Science Reviews* 27.3-4, pp. 365–390. doi: 10.1016/j.quascirev.2007.11.011.

Hernandez-Moreno, C., F. Speranza, and A. Di Chiara (2014). "Understanding kinematics of intra-arc transcurrent deformation: Paleomagnetic evidence from the Liquiñe-Ofqui fault zone (Chile, 38-41°S)". *Tectonics* 33.10, pp. 1964–1988. doi: 10.1002/2014tc003622.

Hickey-Vargas, R., H. Moreno Roa, L. Lopez Escobar, and F. A. Frey (1989). "Geochemical variations in Andean basaltic and silicic lavas from the Villarrica-Lanin volcanic chain (39.5°S): an evaluation of source heterogeneity, fractional crystallization and crustal assimilation". *Contributions to Mineralogy and Petrology* 103.3, pp. 361–386. doi: 10.1007/bf00402922.

Hulton, N., R. Purves, R. McCulloch, D. Sugden, and M. Bentley (2002). "The Last Glacial Maximum and deglaciation in southern South America". *Quaternary Science Reviews* 21.1-3, pp. 233–241. doi: 10.1016/s0277-3791(01)00103-2.

Lara, L. E., J. A. Naranjo, and H. Moreno Roa (2004). "Lanín volcano (39.5°S), Southern Andes: geology and morphostructural evolution". *Revista geológica de Chile* 31.2. doi: 10.4067/s0716-02082004000200004.

Le Maitre, R., A. Streckeisen, B. Zanettin, M. Le Bas, B. Bonin, and P. Bateman (2002). "Igneous rocks: A classification and glossary of terms; Recommendations of the International Union of Geological Sciences". *Subcommission on the Systematics of Igneous rocks*. Cambridge University Press. doi: 10.1017/cbo9780511535581.

López-Escobar, L., J. Cembrano, and H. Moreno Roa (1995). "Geochemistry and tectonics of the Chilean Southern Andes basaltic Quaternary volcanism (37-46°S)". *Revista Geológica de Chile* 22.2, pp. 219–234. doi: http://dx.doi.org/10.5027/andgeoV22n2-a06.

Lorenz, V. (1986). "On the growth of maars and diatremes and its relevance to the formation of tuff rings". *Bulletin of Volcanology* 48.5, pp. 265–274. doi: 10.1007/bf01081755.

Lowell, T. V., C. J. Heusser, B. G. Andersen, P. I. Moreno, A. Hauser, L. E. Heusser, C. Schluchter, D. R. Marchant, and G. H. Denton (1995). "Interhemispheric Correlation of Late Pleistocene Glacial Events". *Science* 269.5230, pp. 1541–1549. doi: 10.1126/science.269.5230.1541.

Macdonald, G. A. (1953). "Pahoehoe, aa, and block lava". *American Journal of Science* 251.3, pp. 169–191. doi: 10.2475/ajs.251.3.169.

Magnall, N., M. R. James, H. Tuffen, and C. Vye-Brown (2017). "Emplacing a Cooling-Limited Rhyolite Lava Flow: Similarities with Basaltic Lava Flows". *Frontiers in Earth Science* 5. doi: 10.3389/feart.2017.00044.

Matthews, J. A. and K. R. Briffa (2005). "The 'little ice age': re-evaluation of an evolving concept". *Geografiska Annaler: Series A, Physical Geography* 87.1, pp. 17–36. doi: 10.1111/j.0435-3676.2005.00242.x.

McGarvie, D. (2009). "Rhyolitic volcano–ice interactions in Iceland". *Journal of Volcanology and Geothermal Research* 185.4, pp. 367–389. doi: 10.1016/j.jvolgeores.2008.11.019.

– (2014). "Glaciovolcanism at Volcán Quetrupillán, Chile". *2014 GSA Annual Meeting in Vancouver, British Columbia*.
McGetchin, T. R., M. Settle, and B. A. Chouet (1974). "Cinder cone growth modeled after Northeast Crater, Mount Etna, Sicily". *Journal of Geophysical Research* 79.23, pp. 3257–3272. doi: 10.1029/jb079i023p03257.
Mee, K., J. S. Gilbert, D. W. McGarvie, J. A. Naranjo, and M. S. Pringle (2009). "Palaeoenvironment reconstruction, volcanic evolution and geochronology of the Cerro Blanco subcomplex, Nevados de Chillán volcanic complex, central Chile". *Bulletin of Volcanology* 71.8, pp. 933–952. doi: 10.1007/s00445-009-0277-7.
Mercer, J. H. (1965). "Glacier Variations in Southern Patagonia". *Geographical Review* 55.3, p. 390. doi: 10.2307/213136.
Moreno Roa, H., L. López-Escobar, and J. Cembrano (1994). "The Villarrica-Quetrupillan-Lanin volcanic chain: a review and probable significance in the Southern Andes, Chile". *Congreso Geologico Chileno*. 7, pp. 339–341.
Moreno Roa, H. and L. Lara (2008). *Geología del área Pucón-Curarrehue: regiones de La Araucanía y de Los Ríos: Regiones de la Araucanía y de los Ríos*. [Map scale 1:100000.]
Moreno, P., T. Lowell, G. J. Jr, and G. Denton (1999). "Abrupt Vegetation and Climate Changes During the Last Glacial Maximumand Last Termination in The Chilean Lake District: A Case Study from Canal De La Puntilla (41oS)". *Geografiska Annaler, Series A: Physical Geography* 81.2, pp. 285–311. doi: 10.1111/j.0435-3676.1999.00059.x.
Pavez, A. (1997). "Geología e historia evolutiva del Complejo Volcánico Quetrupillán, Andes del Sur, 39, 5° S". *VIII Congreso Geológico Chileno*. Vol. 2, pp. 1443–1447. [In Spanish].
Petit-Breuilh Sepúlveda, M. E. (2004). *La historia eruptiva de los volcanes hispanoamericanos (siglos XVI al XX)*. Cabildo Insular de Lanzarote. [In Spanish].
Rawson, H., J. A. Naranjo, V. C. Smith, K. Fontijn, D. M. Pyle, T. A. Mather, and H. Moreno Roa (2015). "The frequency and magnitude of post-glacial explosive eruptions at Volcán Mocho-Choshuenco, southern Chile". *Journal of Volcanology and Geothermal Research* 299, pp. 103–129. doi: 10.1016/j.jvolgeores.2015.04.003.
Rosenau, M., D. Melnick, and H. Echtler (2006). "Kinematic constraints on intra-arc shear and strain partitioning in the southern Andes between 38°S and 42°S latitude". *Tectonics* 25.4. doi: 10.1029/2005tc001943.
Schonwalder-Angel, D., J. A. Cortés, and E. S. Calder (2018). "The interplay of magmatism and tectonics: An example based on the satellite scoria cones at Llaima volcano, Chile". *Journal of Volcanology and Geothermal Research* 367, pp. 31–45. doi: 10.1016/j.jvolgeores.2018.10.020.
Servicio Nacional de Geología y Minería (2013). *Mapa Preliminar de Peligros del Volcán Quetrupillán*. url: http://sitiohistorico.sernageomin.cl/pdf/rnvv/Quetrupillan.pdf.
– (2019). *Complejo Volcánico Quetrupillán*. url: https://www.sernageomin.cl/complejo-volcanico-quetrupillan/.
Sparks, R., H. Pinkerton, and G. Hulme (1976). "Classification and formation of lava levees on Mount Etna, Sicily". *Geology* 4.5, p. 269. doi: 10.1130/0091-7613(1976)4<269:cafoll>2.0.co;2.
Stern, C. R. (2004). "Active Andean volcanism: its geologic and tectonic setting". *Revista geológica de Chile* 31.2. doi: 10.4067/s0716-02082004000200001.
Sumner, J. M. (1998). "Formation of clastogenic lava flows during fissure eruption and scoria cone collapse: the 1986 eruption of Izu-Oshima Volcano, eastern Japan". *Bulletin of Volcanology* 60.3, pp. 195–212. doi: 10.1007/s004450050227.
Sun, M. (2001). "Geochemical variation among small eruptive centers in the central SVZ of the Andes : an evaluation of subduction, mantle and crustal influences". PhD thesis. Florida International University. doi: 10.25148/etd.fi15071601.
Tatsumi, Y. (2005). "The subduction factory: How it operates in the evolving Earth". *GSA Today* 15.7, p. 4. doi: 10.1130/1052-5173(2005)015[4:tsfhio]2.0.co;2.
Tibaldi, A. (1995). "Morphology of pyroclastic cones and tectonics". *Journal of Geophysical Research: Solid Earth* 100.B12, pp. 24521–24535. doi: 10.1029/95jb02250.
Toloza, V. (2015). "Tefroestratigrafía postglacial del Complejo Volcánico Quetrupillán 39° 30'S, 71° 43'O. Regiones de La Araucanía y de Los Ríos, Chile." Universidad de Concepción.
Tuffen, H., M. R. James, J. M. Castro, and C. I. Schipper (2013). "Exceptional mobility of an advancing rhyolitic obsidian flow at Cordón Caulle volcano in Chile". *Nature Communications* 4.1. doi: 10.1038/ncomms3709.
Valdivia Muñoz, P. A. (2016). "Estudio petrológico y geoquímico del volcán Huililco, IX Región, Chile". Universidad de Chile.
Valentine, G. A. and C. B. Connor (2015). "Basaltic Volcanic Fields". *The Encyclopedia of Volcanoes*. Elsevier, pp. 423–439. doi: 10.1016/b978-0-12-385938-9.00023-7.
Witter, J. B., V. C. Kress, P. Delmelle, and J. Stix (2004). "Volatile degassing, petrology, and magma dynamics of the Villarrica Lava Lake, Southern Chile". *Journal of Volcanology and Geothermal Research* 134.4, pp. 303–337. doi: 10.1016/j.jvolgeores.2004.03.002.
Wohletz, K. H. and M. F. Sheridan (1983). "Hydrovolcanic explosions; II, Evolution of basaltic tuff rings and tuff cones". *American Journal of Science* 283.5, pp. 385–413. doi: 10.2475/ajs.283.5.385.